Simulations of A-RNA Duplexes. The Effect of Sequence, Solute Force Field, Water Model, and Salt Concentration

ARTICLE *in* THE JOURNAL OF PHYSICAL CHEMISTRY B · JULY 2012

Impact Factor: 3.3 · DOI: 10.1021/jp3014817 · Source: PubMed

6 AUTHORS, INCLUDING:

Petra Kührová
Palacký University of Olomouc
13 PUBLICATIONS **190** CITATIONS

SEE PROFILE

Michal Otyepka
Palacký University of Olomouc
180 PUBLICATIONS **4,542** CITATIONS

SEE PROFILE

THE JOURNAL OF PHYSICAL CHEMISTRY B

Article

pubs.acs.org/JPCB

Simulations of A-RNA Duplexes. The Effect of Sequence, Solute Force Field, Water Model, and Salt Concentration

Ivana Beššeová,[†] Pavel Banáš,[†,‡] Petra Kührová,[‡] Pavlína Košinová,[‡] Michal Otyepka,[†,‡] and Jiří Šponer*[,†,§]

[†]Institute of Biophysics, Academy of Sciences of the Czech Republic, Kralovopolska 135, 612 65 Brno, Czech Republic

[‡]Regional Centre of Advanced Technologies and Materials, Department of Physical Chemistry, Faculty of Science, Palacky University, tr. 17 listopadu 12, 771 46, Olomouc, Czech Republic

[§]CEITEC - Central European Institute of Technology, Campus Bohunice, Kamenice 5, 625 00 Brno, Czech Republic

Supporting Information

ABSTRACT: We have carried out an extended reference set of explicit solvent molecular dynamics simulations (63 simulations with 8.4 μs of simulation data) of canonical A-RNA duplexes. Most of the simulations were done using the latest variant of the Cornell et al. AMBER RNA force field bsc0χ_{OL3}, while several other RNA force fields have been tested. The calculations show that the A-RNA helix compactness, described mainly by geometrical parameters inclination, base pair roll, and helical rise, is sequence-dependent. In the calculated set of structures, the inclination varies from 10° to 24°. On the basis of simulations with modified bases (inosine and 2,6-diaminopurine), we suggest that the sequence-dependence of purely canonical A-RNA double helix is caused by the steric shape of the base pairs, i.e., the van der Waals interactions. The electrostatic part of stacking does not appear to affect the A-RNA shape. Especially visible is the role of the minor groove amino group of purines. This resembles the so-called Dickerson−Calladine mechanical rules suggested three decades ago for the DNA double helices. We did not identify any long-living backbone substate in A-RNA double helices that would resemble, for example, the B-DNA BI/BII dynamics. The variability of the A-RNA compactness is due to mutual movements of the consecutive base pairs coupled with modest change of the glycosidic χ torsion. The simulations further show that the A-RNA compactness is modestly affected by the water model used, while the effect of ionic conditions, investigated in the range from net-neutral condition to ~0.8 M monovalent ion excess salt, is smaller.

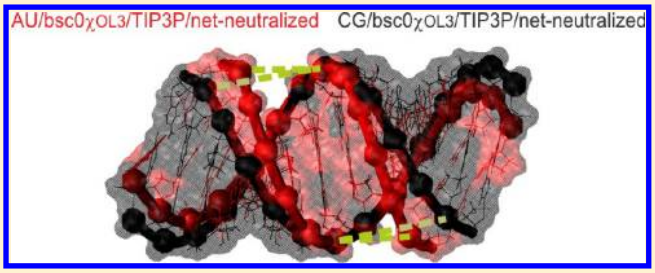

INTRODUCTION

DNA and RNA duplexes are highly negatively charged polymers that are extensively hydrated and surrounded by counterions atmosphere under physiological conditions. Therefore, their structural and dynamical features may be affected by ionic conditions.[1−9] Noncanonical quadruplex DNA and folded RNA molecules formed by complex hierarchy of molecular building blocks[10−12] are even more sensitive to ionic conditions than the duplexes.[13−19] Various aspects of ion binding to nucleic acids and effects of ion binding on nucleic acid structure have been studied by diverse experimental techniques.[9,13,14,17−20] However, as extensively discussed in the literature,[17,18,21−23] experimental techniques to study ion binding to nucleic acids face some limitations, and thus the present knowledge of cation−nucleic acid interactions is far from being complete. In this respect, atomistic molecular dynamics (MD) simulations may provide useful complementary information to the results of experimental techniques.[24−46] In general, MD simulations are able to deliver valuable data about structural dynamics of nucleic acids.[47−51] Contemporary simulations are obviously based on many approximations, which limit their predictive power in studies of structural dynamics of nucleic acids and ion binding to nucleic acids. Besides the substantial force field approximations (use of simple nonpolarizable effective pair additive potentials), there are some others, such as the finite (and rather small) size of simulation boxes, particle mesh Ewald technique accounting for electrostatic interactions under used periodic boundary conditions, and so forth.[32,52,53] These approximations may complicate straightforward comparison of experimental and simulation salt conditions.[52,54,55] Accurate description of divalent ions such as Mg^{2+} is rather outside the applicability of simple nonpolarizable force fields.[22,32,56] On the other hand, simulations can provide valuable qualitative insights and predictions of specific monovalent ion binding sites, although in some cases the inability of MD to describe such ion binding sites was also reported.[30]

Received: February 14, 2012
Revised: June 29, 2012
Published: July 18, 2012

There is an increasing evidence that models of water might also impact structural dynamics of the simulated biomolecules,[57−62] although no systematic analysis has been made for canonical A-RNA helices. There are several simple rigid models of water molecules that can be used for nucleic acids simulations, such as TIPnP[63−65] models and SPC/E.[66] Three-site water models are preferably used in simulations of nucleic acids due to their relatively low computational cost compared to more-site models.[60] For nucleic acid simulations, the most frequently used water models are TIP3P and SPC/E. Comparing the TIP3P and SPC/E parameters, the SPC/E water has larger diameter (σ) and H−O−H angle.[60] The self-diffusion coefficient for the TIP3P model is much larger than that for the SPC/E model, which is closer to the experimental data.[67] The overestimated mobility of the TIP3P model increases the speed of the sampling of the molecules. Decreased specificity of solvation has been reported in simulations of short protein hairpin for the SPC/E and TIP3P water models compared to the TIP5P model providing more accurate values of pure water properties.[57,60] The difference in water model significantly influenced the structural dynamics of the unstructured part of the protein, while the dynamics of the structured part was similar for all three water models.[60]

A few years ago, we carried out a set of reference 50-ns-long simulations of three A-RNA double helices.[68] We compared two at that time standard variants of the Cornell et al.[69] AMBER force field for RNA, i.e., *ff*99[70] and *ff*99bsc0,[71] and two different simulation environments, net-neutralization with Na^+ (c(Na^+) ∼0.18 M) and the TIP3P water model[63] and excess salt (∼0.12 M) KCl with the SPC/E water model.[66] The A-RNA structure showed surprising sequence dependence, mainly considering the compactness of the A-RNA double-helix, as described by the mutually coupled parameters base pair inclination and base pair roll. In the A-RNA duplex, the base pair roll arises upon helical twisting when the base pairs are inclined with respect to the helix axis.[72−76] Basically, the parameter inclination defined in a global helix axis coordinate system corresponds to the parameter base pair roll in a local (wedge) coordinate system (cf. Figure 1 in ref 74, which also provides the corresponding mathematical equations). Thus the larger inclination inevitably leads to the larger base pair roll.[74−76] Increase of inclination is also associated with narrowing of the major groove and reduction of helical rise, making the duplex more compact.[68] We found also modest difference between the tested solute force fields (with *ff*99bsc0 giving more compact A-RNA helix) and modest effect of the environment (solvent+salt), which we tentatively attributed to more efficient screening of the phosphate−phosphate repulsion in excess salt simulations. The magnitude of the force field and environments effects was found to be sequence-dependent, being significant for alternating $(CG)_n$ duplex and barely noticeable for $(UA)_n$ duplex. Despite the observed effects of force field and salt environments, we suggested that all tested simulation conditions appear suitable for A-RNA description. The reason is the large variability of A-RNA geometries seen in available X-ray structures, which precludes one from establishing unambiguous reference values for the A-RNA helix geometry parameters.[68]

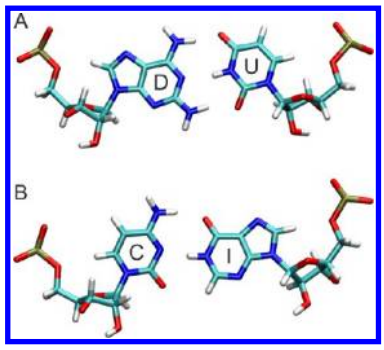

Figure 1. (A) diaminopurine/uracil and (B) cytosine/inosine base pairs.

However, several new findings emerged after publishing the above-mentioned study. First, it has been shown that both *ff*99 and *ff*99bsc0 force fields tend to irreversibly degrade RNA structures. Irreversible transitions to unexpectedly open and under-twisted structures with χ glycosidic angle shifted to the high-*anti* territory were observed in longer simulations.[77] These structures, resembling a ladder, have not been observed experimentally. It should be noted that ladder-like structures certainly affected some earlier RNA MD studies, e.g., simulations of small stem-loop hairpin systems. Although the formation of ladders has not been acknowledged in the earlier literature, it sometimes can be recognized from the published figures.[78] The revelation of ladder-like transitions in RNA simulations has prompted reparameterization of the χ dihedral profile, known as the χ_{OL3} (originally marked as χ_{OL}) force field.[78,79] This is now the standard AMBER force field for RNA simulations in combination with the earlier bsc0 α/γ reparameterization, since there is synergy between these two independent dihedral term refinements. Second, analysis of the structural flexibility of RNA reverse-kink-turns revealed visible sensitivity of the RNA structural dynamics and structures derived by the simulations to the environment.[61] Closer inspection of the data led to the unexpected suggestion that the sensitivity of RNA dynamics was primarily due to water model differences, while type and concentration of ions appeared to play much smaller roles. Although this result might at first glance seem surprising, some coupling between the physical-chemistry properties of the water model and the solute dynamics is definitely possible.[60,80] It is because the number of water particles interacting with the solute is much larger than the number of interacting ions. For example, due to the exposure of anionic phosphates to the hydration, the water model may affect their structural dynamics. This in turn can influence the behavior of the highly correlated torsion angles along the backbone chains and the overall RNA structural dynamics and structures derived by the simulations.

The new findings prompted us to carry out a major extension (more than 60 individual 50−500-ns simulation runs, resulting in ∼9 μs of simulation data in total) of our earlier study on A-RNA duplexes, with three basic aims; (i) to understand the origin of the sequence-dependency of the A-RNA structure; (ii) to depict the effect of force field, and (iii) to dissect the influence of the water model and ion type on the simulation behavior. We first investigated the effect of sequence on A-RNA structure, using a set of 10 different either alternating complementary $r(YR)_7{\cdot}r(YR)_7$ (abbreviated further as $(YR)_7$) or homopurine $(R)_{14}$ Watson−Crick duplexes (Y = pyrimidine; R = purine). The *ff*99bsc0+χ_{OL3} force field with two water+salt environments was used. The simple repetitive sequences allow one to magnify the sequence effects, so they can be more easily detected. Besides using canonical nucleotides (A, C, G, and U), we also included sequences with inosine (I) and 2,6-

dx.doi.org/10.1021/jp3014817 | J. Phys. Chem. B 2012, 116, 9899−9916

Table 1. List of the AMBER Simulations and Set of Conditions Used in the Study[a]

simulation (sequence)	length [ns]	force field	ions	concentration of M^+/Cl^-[b]	water box
CG-tract $(CG)_7$					
CG_χ_{OL3}-Na-TIP3P	500	*ff*99bsc0χ_{OL3}	Na^+	0.18 M/0.0 M (NN)	TIP3P
CG_χ_{OL3}-KCl-SPCE	500	*ff*99bsc0χ_{OL3}	K^+, Cl^-	0.3 M/0.12 M (ESC0.12)	SPC/E
CG_χ_{OL3}-K-TIP3P	200	*ff*99bsc0χ_{OL3}	K^+	0.18 M/0.0 M (NN)	TIP3P
CG_χ_{OL3}-KCl-TIP3P	200	*ff*99bsc0χ_{OL3}	K^+, Cl^-	0.3 M/0.12 M (ESC0.12)	TIP3P
CG_χ_{OL3}-Na-SPCE	50	*ff*99bsc0χ_{OL3}	Na^+	0.18 M/0.0 M (NN)	SPC/E
CG_χ_{OL3}-K-SPCE	50	*ff*99bsc0χ_{OL3}	K^+	0.18 M/0.0 M (NN)	SPC/E
CG_χ_{OL3}-NaCl-TIP3P	50	*ff*99bsc0χ_{OL3}	Na^+, Cl^-	0.3 M/0.12 M (ESC0.12)	TIP3P
CG_χ_{OL3}-NaCl-SPCE	50	*ff*99bsc0χ_{OL3}	Na^+, Cl^-	0.3 M/0.12 M (ESC0.12)	SPC/E
CG_χ_{OL3}-K-TIP3P-Jorg	200	*ff*99bsc0χ_{OL3}	K^+	0.18 M/0.0 M (NN)[c]	TIP3P
CG_χ_{OL3}-K-TIP3P-Roux	200	*ff*99bsc0χ_{OL3}	K^+	0.18 M/0.0 M (NN)[d]	TIP3P
CG_χ_{OL3}-KCl-TIP3P-Jorg	200	*ff*99bsc0χ_{OL3}	K^+, Cl^-	0.3 M/0.12 M (ESC0.12)[c]	TIP3P
CG_χ_{OL3}-KCl-TIP3P-Roux	200	*ff*99bsc0χ_{OL3}	K^+, Cl^-	0.3 M/0.12 M (ESC0.12)[d]	TIP3P
CG_χ_{OL3}-KCl-TIP3P-ESC0.32	200	*ff*99bsc0χ_{OL3}	K^+, Cl^-	0.5 M/0.32 M (ESC0.32)	TIP3P
CG_χ_{OL3}-KCl-TIP3P-ESC0.52	200	*ff*99bsc0χ_{OL3}	K^+, Cl^-	0.7 M/0.52 M (ESC0.52)	TIP3P
CG_χ_{OL3}-KCl-TIP3P-Jorg-ESC0.52	200	*ff*99bsc0χ_{OL3}	K^+, Cl^-	0.7 M/0.52 M (ESC0.52)[c]	TIP3P
CG_χ_{OL3}-KCl-TIP3P-Roux-ESC0.52	200	*ff*99bsc0χ_{OL3}	K^+, Cl^-	0.7 M/0.52 M (ESC0.52)[d]	TIP3P
CG_χ_{OL3}-KCl-TIP3P-ESC0.82	200	*ff*99bsc0χ_{OL3}	K^+, Cl^-	1.0 M/0.82 M (ESC0.82)	TIP3P
BRNA_χ_{OL3}-Na-TIP3P[e]	50	*ff*99bsc0χ_{OL3}	Na^+	0.18 M/0.0 M (NN)	TIP3P
BRNA_χ_{OL3}-KCl-SPCE[e]	50	*ff*99bsc0χ_{OL3}	K^+, Cl^-	0.3 M/0.12 M (ESC0.12)	SPC/E
CG(ESC0.12)_χ_{OL3}-Na-TIP3P[f]	50	*ff*99bsc0χ_{OL3}	Na^+	0.18 M/0.0 M (NN)	TIP3P
CG(NN)_χ_{OL3}-KCl-SPCE[g]	50	*ff*99bsc0χ_{OL3}	K^+, Cl^-	0.3 M/0.12 M (ESC0.12)	SPC/E
AU-tract $(AU)_7$					
AU_χ_{OL3}-Na-TIP3P	200	*ff*99bsc0χ_{OL3}	Na^+	0.18 M/0.0 M (NN)	TIP3P
AU_χ_{OL3}-KCl-SPCE	200	*ff*99bsc0χ_{OL3}	K^+, Cl^-	0.3 M/0.12 M (ESC0.12)	SPC/E
GA-tract $(GA)_7$					
GA_χ_{OL3}-Na-TIP3P	200	*ff*99bsc0χ_{OL3}	Na^+	0.18 M/0.0 M (NN)	TIP3P
GA_χ_{OL3}-KCl-SPCE	200	*ff*99bsc0χ_{OL3}	K^+, Cl^-	0.3 M/0.12 M (ESC0.12)	SPC/E
GU-tract $(GU)_7$					
GU_χ_{OL3}-Na-TIP3P	200	*ff*99bsc0χ_{OL3}	Na^+	0.18 M/0.0 M (NN)	TIP3P
GU_χ_{OL3}-KCl-SPCE	200	*ff*99bsc0χ_{OL3}	K^+, Cl^-	0.3 M/0.12 M (ESC0.12)	SPC/E
G-tract $(G)_{14}$					
G_χ_{OL3}-Na-TIP3P	200	*ff*99bsc0χ_{OL3}	Na^+	0.18 M/0.0 M (NN)	TIP3P
G_χ_{OL3}-KCl-SPCE	200	*ff*99bsc0χ_{OL3}	K^+, Cl^-	0.3 M/0.12 M (ESC0.12)	SPC/E
A-tract $(A)_{14}$					
A_χ_{OL3}-Na-TIP3P	200	*ff*99bsc0χ_{OL3}	Na^+	0.18 M/0.0 M (NN)	TIP3P
A_χ_{OL3}-KCl-SPCE	200	*ff*99bsc0χ_{OL3}	K^+, Cl^-	0.3 M/0.12 M (ESC0.12)	SPC/E
DU-tract $(DU)_7$					
DU_χ_{OL3}-Na-TIP3P	200	*ff*99bsc0χ_{OL3}	Na^+	0.18 M/0.0 M (NN)	TIP3P
DU_χ_{OL3}-KCl-SPCE	200	*ff*99bsc0χ_{OL3}	K^+, Cl^-	0.3 M/0.12 M (ESC0.12)	SPC/E
D-tract $(D)_{14}$					
D_χ_{OL3}-Na-TIP3P	50	*ff*99bsc0χ_{OL3}	Na^+	0.18 M (NN)	TIP3P
D_χ_{OL3}-KCl-SPCE	50	*ff*99bsc0χ_{OL3}	K^+, Cl^-	0.3 M/0.12 M (ESC0.12)	SPC/E
CI-tract $(CI)_7$					
CI_χ_{OL3}-Na-TIP3P	200	*ff*99bsc0χ_{OL3}	Na^+	0.18 M/0.0 M (NN)	TIP3P
CI_χ_{OL3}-KCl-SPCE	200	*ff*99bsc0χ_{OL3}	K^+, Cl^-	0.3 M/0.12 M (ESC0.12)	SPC/E
I-tract $(I)_{14}$					
I_χ_{OL3}-Na-TIP3P	50	*ff*99bsc0χ_{OL3}	Na^+	0.18 M/0.0 M (NN)	TIP3P
I_χ_{OL3}-KCl-SPCE	50	*ff*99bsc0χ_{OL3}	K^+, Cl^-	0.3 M/0.12 M (ESC0.12)	SPC/E
2R20[h]					
2R20_ff99-Na-TIP3P	50	*ff*99	Na^+	0.18 M/0.0 M (NN)	TIP3P
2R20_ff99-KCl-SPCE	50	*ff*99	K^+, Cl^-	0.3 M/0.12 M (ESC0.12)	SPC/E
2R20_bsc0-Na-TIP3P	50	*ff*99bsc0	Na^+	0.18 M/0.0 M (NN)	TIP3P
2R20_bsc0-KCl-SPCE	50	*ff*99bsc0	K^+, Cl^-	0.3 M/0.12 M (ESC0.12)	SPC/E
2R20_χ_{OL3}-Na-TIP3P	50	*ff*99bsc0χ_{OL3}	Na^+	0.18 M/0.0 M (NN)	TIP3P
2R20_χ_{OL3}-KCl-SPCE	50	*ff*99bsc0χ_{OL3}	K^+, Cl^-	0.3 M/0.12 M (ESC0.12)	SPC/E
2R20_ff99-Na-TIP3P-χ_{Ode}	50	*ff*99χ_{Ode}	Na^+	0.18 M/0.0 M (NN)	TIP3P
2R20_bsc0-Na-TIP3P-χ_{Ode}	50	*ff*99bsc0χ_{Ode}	Na^+	0.18 M/0.0 M (NN)	TIP3P
2R20_ff99-Na-TIP3P-χ_{Yil}	50	*ff*99χ_{Yil}	Na^+	0.18 M/0.0 M (NN)	TIP3P

dx.doi.org/10.1021/jp3014817 | *J. Phys. Chem. B* 2012, 116, 9899−9916

Table 1. continued

simulation (sequence)	length [ns]	force field	ions	concentration of M^+/Cl^- [b]	water box
2R20[h]					
2R20_ff99-KCl-SPCE-χ_{Yil}	50	*ff*99χ_{Yil}	K^+, Cl^-	0.3 M/0.12 M (ESC0.12)	SPC/E
2R20_bsc0-KCl-SPCE-χ_{Yil}	50	*ff*99bsc0χ_{Yil}	K^+, Cl^-	0.3 M/0.12 M (ESC0.12)	SPC/E
1QC0[i]					
1QC0_χ_{OL3}-Na-TIP3P	50	*ff*99bsc0χ_{OL3}	Na^+	0.18 M/0.0 M (NN)	TIP3P
1QC0_χ_{OL3}-KCl-SPCE	50	*ff*99bsc0χ_{OL3}	K^+, Cl^-	0.3 M/0.12 M (ESC0.12)	SPC/E
1QC0_ff99-Na-TIP3P-χ_{Yil}	50	*ff*99χ_{Yil}	Na^+	0.18 M/0.0 M (NN)	TIP3P
1QC0_ff99-KCl-SPCE-χ_{Yil}	50	*ff*99χ_{Yil}	Na^+	0.18 M/0.0 M (NN)	TIP3P
1QC0_bsc0-KCl-SPCE-χ_{Yil}	50	*ff*99bsc0χ_{Yil}	K^+, Cl^-	0.3 M/0.12 M (ESC0.12)	SPC/E

[a]The name of the simulation is composed of five parts: i.e., either the tract sequence or the pdb code of the X-ray structure_basic force field−ions−water model−alternative χ correction (if any)−alternative ion parameters (if any). The CHARMM simulations are summarized in Supporting Information I (Table S13). NN = net-neutral condition; ESC = excess salt condition, the number indicates molar concentration of anions, i.e., the added excess salt. Cheatham et al. ion parameters used if not specified otherwise. [b]The two listed values represent total concentration of cations/anions (i.e, excess salt). [c]The Jorgensen et al. ion parameters were used. [d]The Roux et al. ion parameters were used. [e]B-form at the start. [f]End of the KCl/SPC/E simulation with 0.12 M added salt taken as the start. [g]End of the Na^+/TIP3P simulation taken as the start. [h]r$(GCGUUUGAAACGC)_2$ with central GG mismatch. [i]Canonical r$(GCACCGUUGG)_2$.

diaminopurine (D). I and D are steric mimics of A and G, respectively, while electrostatically they conversely mimic G and A, respectively.[81,82] These non-natural bases were commonly used in the past to address the sequence-dependency of B-DNA structure, using both experimental[83,84] and simulation approaches.[85] Furthermore, we carry out a set of simulations comparing different water models and different ion types/concentrations for the $(CG)_7$ alternating duplex, since this sequence shows the largest sensitivity of its structure to the water+salt models. The $(CG)_7$ duplex has also been used to verify the convergence of the simulations using 0.5 μs control runs. To prove the lack of influence of starting structure on A-RNA simulations, we performed simulations showing a spontaneous transition of the duplex from B-RNA to A-RNA form and multiple simulations using different A-RNA starting geometries. In all cases, the helical parameters of the simulated molecule rather swiftly adopted the expected values for given salt+water model settings, independently of the starting geometry. Finally, we report a set of simulations using two common RNA sequences to test the effect of the RNA force field, considering several force field modifications available in the literature, including eight simulations carried out with the CHARMM force field.[86,87] For some other recent studies of canonical A-RNA duplexes (dealing specifically with harmonic stiffness of RNA and DNA double helices), see refs 51, 56, and 88.

METHODS

The present study is primarily based on 55 explicit solvent MD simulations of A-RNA duplexes with the AMBER 10.0 package.[89] Canonical A-RNA helices composed of 14 base pairs with 10 different sequences were simulated (Table 1). C, G, A, U, diaminopurine (D), and inosine (I) nucleotides were used in the 14-mers (Figure 1). The starting structures containing canonical Watson−Crick (WC) base pairs were built by the INSIGHT II program package (Biosym/MSI, San Diego, CA, October 1995). D and I were paired with U and C, respectively.

The diaminopurine and inosine residues were prepared in the XLEaP program.[89] We used the Hartree−Fock method with the 6-31G* basis set to optimize their geometries and to calculate the electrostatic potential in the Gaussian09 program.[90] The RESP charges required in MD simulations were generated in ANTECHAMBER.[91] The complete list of RESP charges for D and I is shown in Supporting Information I. The starting structure of $(CG)_7$ RNA in B-DNA conformation was prepared with the INSIGHT II program package (Biosym/MSI, San Diego, CA, October 1995). Beside these helices, two solution models of duplex RNA starting from their published crystal structure[92,93] were explored (see below).

Each helix was put into the truncated octahedral solvation box of either TIP3P[63] or SPC/E[66] water molecules (Table 1). Na^+ (TIP3P: r = 1.369 Å, ε = 0.0874 kcal mol^{-1}; SPC/E: r = 1.212 Å, ε = 0.3526 kcal mol^{-1})[94] or K^+ (TIP3P: r = 1.705 Å, ε = 0.1936 kcal mol^{-1}; SPC/E: r = 1.593 Å, ε = 0.4297 kcal mol^{-1})[94] ions were used to neutralize the RNA structures. The excess salt simulations were performed by the addition of Cl^- ions (TIP3P: r = 2.513 Å, ε = 0.0355 kcal mol^{-1}; SPC/E: r = 2.711 Å, ε = 0.0127 kcal mol^{-1})[94] and appropriate cations. The XLEaP modul of AMBER package[89] was used to solvate and to place ions to the starting structures. We further carried out some additional simulations by using two additional sets of parameters for K^+ and Cl^- and combined them with the TIP3P water model, i.e., Jorgensen et al. set: K^+ (r = 2.756 Å, ε = 0.0005 kcal mol^{-1}),[95] Cl^- (r = 2.228 Å, ε = 0.7100 kcal mol^{-1})[95] and Roux et al.; K^+ (r = 1.764 Å, ε = 0.0870 kcal mol^{-1}),[96] Cl^- (TIP3P: r = 2.270 Å, ε = 0.1500 kcal mol^{-1}).[96]

The protocol for minimization and equilibration was as follows: After 5000 steps of minimization and short MD (200 ps) of water molecules and ions, two series of minimizations (1000 steps) and MD (20 ps) were carried out while applying positional restraints with force constants of 50 and 25 kcal mol^{-1} Å^{-2} to the solute atoms. Subsequently, five rounds of minimization of 1000 steps were performed with restraints having stepwise decreasing values of force constant (20, 15, 10, 5, and 0 kcal mol^{-1} Å^{-2}) applied to the RNA atoms. After that, the system was heated from 50 to 300 K during unrestrained 100-ps long MD simulation.

Most simulations were performed using the PMEMD code[97] of AMBER 10[89] with *ff*99bsc0 force field[71] and χ_{OL3} correction, substantially improving the description of *anti*/high-*anti* and *syn* regions of the glycosidic χ torsion angle.[78] The *ff*99bsc0+χ_{OL3} parameter set is the current default for RNA in the AMBER package (accessible, e.g., as part of the current AMBER *ff*10 set of biomolecular force fields). In addition, we used the *ff*99 force field[70] as well as two alternative modifications of the χ profile, those of Yildirim et al.[98] (abbreviated as χ_{Yil}) and Ode et al.[99] (χ_{Ode}), which can be found in the literature.

dx.doi.org/10.1021/jp3014817 | J. Phys. Chem. B 2012, 116, 9899−9916

Table 2. The Representative Mean Structural Parameters, Dihedral Angles, P...P Distances of the 10 Studied 14-mer Tracts Calculated for the Inner 10 Base Pair Segments over 200-ns-Long Simulations (Table 1) When Using Net-Neutral (NN) Conditions and Excess (ESC0.12) Salt[a]

NN/Na^+/TIP3P	A-tract	I-tract	AU-tract	CG-tract	CI-tract	DU-tract	G-tract	D-tract	GA-tract	GU-tract
twist [°]	29.0	28.8	29.6	29.6	29.0	30.4	29.5	29.5	29.9	30.1
roll [°]	10.4	10.0	10.7	5.5	13.5	7.8	7.0	7.8	7.5	8.9
slide [Å]	−1.57	−1.57	−1.43	−1.90	−1.05	−1.82	−1.92	−1.90	−1.72	−1.55
inclination [°]	19.3	18.9	18.8	10.0	23.8	13.5	13.2	14.5	13.8	15.9
h-rise [Å]	2.55	2.58	2.54	2.95	2.49	2.67	2.76	2.69	2.72	2.69
propeller [°]	−10.8	−11.2	−15.8	−8.4	−14.7	−14.7	−7.5	−8.1	−11.4	−14.3
pucker [°]	18.3	19.3	17.8	14.6	18.4	15.2	15.2	15.9	16.0	16.2
χ [°]	203.1	202.8	204.8	197.5	208.4	199.3	197.3	198.1	199.5	202.3
α [°]	−74.5	−74.9	−75.7	−72.1	−76.6	−74.2	−73.8	−74.2	−74.3	−74.9
β [°]	173.9	173.3	173.6	173.6	173.3	173.9	174.3	174.6	173.1	173.3
γ [°]	63.7	63.9	63.6	64.3	63.4	63.5	63.8	63.8	64.3	63.9
δ [°]	78.8	79.2	79.0	78.3	78.6	78.1	77.6	78.7	78.3	78.7
ε [°]	201.5	201.4	201.8	201.4	202.1	202.1	201.7	201.5	201.4	201.9
ζ [°]	−68.9	−68.6	−68.5	−68.3	−68.8	−67.3	−68.0	−68.8	−68.1	−68.1
P...P [Å]	13.1	13.7	11.7	16.1	10.8	11.5	14.2	13.6	13.9	12.3
ESC0.12/KCl/SPC/E	A-tract	I-tract	AU-tract	CG-tract	CI-tract	DU-tract	G-tract	D-tract	GA-tract	GU-tract
twist [°]	29.0	29.3	30.0	31.3	30.2	31.1	29.9	29.7	30.1	30.5
roll [°]	11.6	12.3	12.3	9.6	13.6	9.5	8.9	9.7	9.2	11.4
slide [Å]	−1.56	−1.47	−1.32	−1.53	−1.02	−1.67	−1.83	−1.83	−1.67	−1.40
inclination [°]	21.3	22.5	21.3	16.6	23.9	16.2	16.5	17.9	16.8	19.9
h-rise [Å]	2.48	2.45	2.47	2.64	2.48	2.56	2.61	2.55	2.60	2.54
propeller [°]	−11.1	−12.6	−16.6	−13.6	−15.2	−16.4	−8.7	−9.0	−11.9	−15.9
pucker [°]	18.6	19.0	17.8	14.1	17.6	14.9	15.3	16.1	16.2	16.4
χ [°]	203.4	204.1	206.0	201.0	208.6	200.8	198.4	199.1	200.4	204.2
α [°]	−75.9	−76.2	−76.3	−74.8	−76.6	−75.1	−74.6	−75.2	−75.0	−75.5
β [°]	174.2	174.1	173.4	173.8	172.5	173.7	174.9	174.9	173.7	173.3
γ [°]	63.2	62.9	63.1	63.5	63.2	62.8	63.0	62.9	63.5	63.0
δ [°]	78.4	79.0	79.0	79.0	79.5	78.1	77.6	78.2	78.1	78.5
ε [°]	201.7	201.9	202.2	202.4	202.1	202.4	202.1	201.8	201.7	202.6
ζ [°]	−68.7	−68.5	−68.3	−67.9	−68.3	−67.3	−68.0	−67.9	−68.1	−68.0
P...P [Å]	11.6	10.9	9.6	11.0	9.8	9.4	11.9	11.7	11.9	9.8

[a]The data for I- and D- tracts were calculated over 50-ns. The graphical representation of the listed values is shown in Figure 3. The error estimation is listed in Table S3 and visualized in Figure S2 in Supporting Information I.

Two systems were also simulated using CHARMM27[86] and CHARMM36,[87] (i.e., CHARMM27 with reparameterized 2′-OH group torsion angle) force fields. We obtained eight trajectories with 1 μs of simulations in total; further details can be found in Supporting Information I.

Simulations were performed under periodic boundary conditions using the particle-mesh Ewald method;[100,101] a 9 Å cut off was applied for Lennard-Jones interactions in NpT ensemble (1 atm and 300 K) using weak-coupling Berendsen thermostat[102] with coupling time of 1 ps. The SHAKE algorithm was applied to all X−H bonds to eliminate the fastest vibrations and to allow a longer integration step, which was 2 fs.

Helical parameters were measured utilizing the 3DNA program.[103] The 3DNA outputs were further processed by in-house scripts. We also analyzed the width of the major groove that we defined as the shortest distance between phosphate atoms in the opposite chains (henceforth abbreviated as P...P), the particular distances are listed for each structure in Supporting Information I (Table S1). Note that the averaged parameters were derived based on analysis of their time-developments along the trajectories and not from averaged structures. The convergence of helical parameters was explicitly tested by comparing results of differently long parts of CG-tract trajectories (50, 200, 250, or 500-ns) as well as by applying the Mann−Kendall test[104] available in the extended version of Microsoft Excel. The Ptraj module of AMBER also helped to carry out additional analyses. We visualized MD productions and produced figures in the VMD program (http://www.ks.uiuc.edu/Research/vmd/).[105]

STARTING STRUCTURES, PERFORMED SIMULATIONS, AND ANALYSIS

First Set of Simulations. To explore the effect of the sequence on the A-RNA duplex structure, the following RNA duplexes with repetitive sequences (tracts) were simulated: $(CG)_7$, $(AU)_7$, $(GA)_7$, $(GU)_7$, $(G)_{14}$, $(A)_{14}$, $(DU)_7$, $(D)_{14}$, $(CI)_7$ and $(I)_{14}$ (Table 1). Note that some alternating tracts start with purine (R) base, while the others with pyrimidine (Y), which leads to a different number of YR and RY steps. This, however, has no significant effect on our results. We varied cations (Na^+ and K^+) and cation concentrations, using net-neutral condition (abbreviated as NN) with ∼0.18 M cation concentration and ∼0.3 M cation/∼0.12 M Cl^- excess salt condition (abbreviated as ESC or ESC0.12). Appropriate Cheatham et al.[94] parameters were used with either the TIP3P or SPC/E water model (Table 1). Each simulation was 50, 200, or 500-ns-long (Table 1).

dx.doi.org/10.1021/jp3014817 | J. Phys. Chem. B 2012, 116, 9899−9916

Second Set of Simulations. On the basis of previous work[68] and the ongoing simulations, we proposed that the CG-tract is most sensitive to the choice of the force field and ionic strength. Thus we carried out more thorough analysis of the $(CG)_7$ helix using different ion/water conditions. Two water models (TIP3P and SPC/E) and three sets of ions parameters (Cheatham et al.,[94] Joergensen et al.,[95] and Roux et al.,[96]) were used, in addition at different concentrations of KCl, ranging from NN condition up to ~0.82 M excess salt (cation concentration $c(K^+)$ ~0.18−1 M) (Table 1). The simulations were 200 long (Table 1).

Third Set of Simulations. We have carried out simulations starting from two different crystallographic data of RNA duplexes (Table 1): (i) 2R20 duplex (pdb code 2R20,[92] resolution 1.30 Å) having palindromic sequence r-$(GCGUUUGAAACGC)_2$, where the central base pair is noncanonical *cis* Watson−Crick/Hoogsteen G/G, and (ii) the first 10 base pairs (residues 101−110 and 129−138 in the X-ray numbering) of 1QC0 structure representing part of the 19-mer of the canonical A-RNA duplex (pdb code 1QC0,[93] resolution 1.55 Å, simulated duplex $r(GCACCGUUGG)_2$).

Fourth Set of Simulations. In order to further test convergence of the simulations, we performed two 200-ns-long simulations of $(CG)_7$ RNA duplex starting from B-RNA geometry (using canonical B-DNA duplex as the template) under the NN ($c(Na^+)$ = 0.18 M, TIP3P) and ESC ($c(K^+)$ = 0.3 M/$c(Cl^-)$ = 0.12 M SPC/E) conditions (Table 1). Additionally, two simulations of CG-tract were carried out (Table 1) by interchanging the salt condition. We run a simulation under NN salt strength using the CG-tract structure averaged over the 199−200-ns period of the ESC simulation ($c(K^+)$ = 0.3 M/$c(Cl^-)$ = 0.12 M, SPC/E), while another simulation was performed under ESC conditions ($c(K^+)$ = 0.3 M/$c(Cl^-)$ = 0.12 M, SPC/E) with the starting geometry taken from the end (199−200-ns average) of the NN simulation ($c(Na^+)$ = 0.18 M, TIP3P).

The base pair steps (tilt, roll, twist, shift and slide), helical (inclination and helical rise), and intrabase pair (propeller) parameters describing the global and local topology of the duplexes were analyzed using the 3DNA program (for precise definition of the parameters, see ref 103). The 3DNA program was used also for monitoring of sugar pucker, dihedral backbone angles, and orientation of the glycosidic angle (χ). We also analyzed the width of the major groove that we defined as the shortest distance between phosphate atoms in the opposite chains (henceforth abbreviated as P...P); the particular distances are listed for each structure in Supporting Information I (Table S1). Note that the averaged parameters were derived based on analysis of their time-developments along the trajectories and not from averaged structures. Due to the increased fluctuations, two terminal base pairs at each end were excluded from the analyses.

Initially, we analyzed the global shape of the helices, i.e., we calculated base pair and base pair step parameters, and P...P distances averaged along the duplexes (using the 10 central base pairs for the 14-mers) for each snapshot (1 ps) separately, for 10-ns windows and for whole 50-ns interval in each 50-ns-long simulation (Table S2 and Figure S1 in Supporting Information I). To capture the structural variations at the level of individual base pairs and base pair steps, the average values for each individual base pair and base pair step parameter, dihedral angle, sugar pucker, and P...P distance over the 40-ns intervals and over whole 200-ns simulations were also calculated. All parameters averaged over the whole simulation (over 200 or 50-ns, respectively, cf. Table 1) are called mean structural parameters in this paper (Tables 2−7).

As the standard deviations commonly given in simulation papers reflect the range of thermal fluctuations in the MD simulations rather than error of the average value, we performed the following standard procedure[50] to estimate the accuracy of each mean structural parameter: We split the data line into 10-ns-long nonoverlapping frames and calculated average values from each frame. Then we calculated standard deviations (std_n) of these average values. The 95-percent confidence interval of the mean value is defined as mean ± t·std_n/sqrt(n), where n is number of averaged frames, t is quantile of the distribution (for 50-ns, 200-ns and 500 simulations, $t_{50\text{-ns}}$ = 2.776, $t_{200\text{-ns}}$ = 2.093, and $t_{500\text{-ns}}$= 2.009). The estimation of errors for the calculated structural parameters, dihedral angles, and P...P distances are shown in Tables S2−6 and Figures S2−3 in Supporting Information I. Such a value expresses how much the individual frames differ, i.e., it reflects the variance between the averaged intervals.

In addition, in many cases we monitored in detail time courses of the individual parameters to clarify that there are no distinct substates present during the simulations. Further, CG-tract simulations (under NN and ESC conditions) were prolonged to 0.5 μs (Table 1). All data indicate that a 50-ns time scale is sufficient to achieve the convergence of our results (Table 7, Figure 2 and Figure S1 in the Supporting Information). The development of all listed structural parameters in 10-ns intervals for each nucleotide, base pair, and base pair step within each 200-ns-long trajectory are available in Supporting Information II and III.

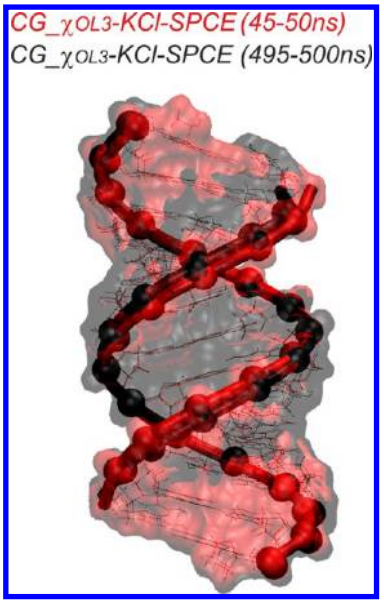

Figure 2. Comparison of CG-tracts averaged over 45−50-ns (red) and 495−500-ns (black). The structures were superimposed via four central base pairs.

RESULTS AND DISCUSSION

Sequence-Dependence of the A-RNA Compactness. For basic analysis of the sequence effects, we used the latest *ff*99bsc0+χ_{OL3}[71,78,79] force field and two ion/water conditions: net-neutralized Na^+ with TIP3P water model (NN) and excess

dx.doi.org/10.1021/jp3014817 | J. Phys. Chem. B 2012, 116, 9899−9916

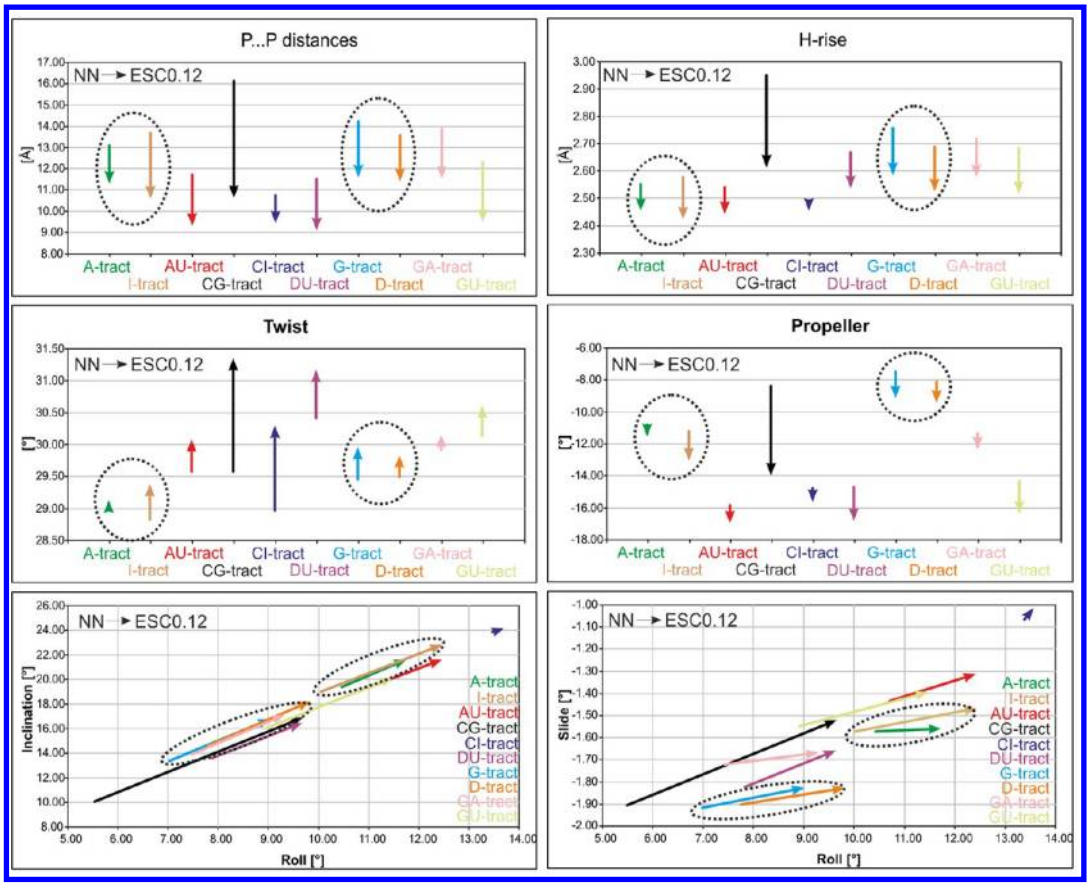

Figure 3. Selected mean structural parameters (and their correlations) for different sequences calculated over 200-ns-long simulations and their shift by applying different salt conditions and solvent models (NN with TIP3P and ESC0.12 with SPC/E). Data for D and I tracts are shown for 50-ns-long simulations. For a given sequence, the starting point of the arrow corresponds to the Na^+/TIP3P simulation while the end point to the KCl/SPC/E simulation. The dotted ellipses mark simulations with similar behavior. See Supporting Information Figure S1 to assess the convergence by comparing 50 and 200-ns data and Supporting Information Figure S2 for the error bars.

salt KCl with the SPC/E water model (ESC0.12, the number 0.12 refers to the ∼0.12 M excess salt concentration; see Methods). These two water/ion conditions are suitable to visualize the differences among the studied sequences and their sensitivity to the environment, as will be further demonstrated below.

The different A-RNA duplexes show different compactness of the helices, which is sequence-dependent and is also sensitive to the water/salt conditions (Figure 3 and Table 2). The compactness of A-RNA is best described by the helical parameter inclination (inclination of base pairs with respect to the helix axis) and base pair step parameter base pair roll. Inclination and roll are mathematically interrelated, as base pair roll arises upon helical twisting when base pairs have inclination, which leads to the roll/inclination correlation[74−76] (Figure 3, see also the Introduction). Increase of inclination is also coupled with narrowing of the major groove, reduction of helical rise, and change in slide.

The impact of varying salt strength/water model follows the same trend, albeit with highly variable magnitude, for all studied sequences. In particular, the ESC0.12 conditions shift the RNA duplexes toward more compact A-RNA with higher roll and inclination. The individual sequences can be characterized by (i) the A-RNA compactness in Na^+/TIP3P conditions and (ii) its change upon changing the simulation condition to the KCl/SPC/E environment (Figure 3 and Table 2). The variations in A-RNA compactness among different simulations are large (Figure 4 and Figure S4 in Supporting Information I). Inclination varies from 10.0° (CG-tract, 200-ns, NN simulation) to 23.9° (CI-tract, 200-ns, ESC0.12 simulation), the coupled parameter base pair roll from 5.5° to 13.6° (the same simulations), propeller twist from −7.4° (G-tract, 200-ns, NN simulation) to −16.5° (AU-tract, 200-ns, ESC0.12 simulation), and so forth.

We wanted to identify other geometrical parameters that are coupled with this roll-inclination movement. However, it appears that the movement is exclusively due to the move of the base pairs, which behave as plates. There is just a small adjustment of the χ angle (with variability of ∼10°) that is coupled to the inclination. The sugar pucker responds neither to the change of the ionic conditions nor the water model (Table 2). There are basically no visible changes of the other dihedral backbone angles. For example, the average α angle changes with solvent/ionic conditions by at most 2.7° (with maximum difference in CG-tract simulations, ESC0.12 vs NN), while $\beta-\zeta$ values do not vary at all (Table 2). We monitored in detail the individual angles in selected trajectories to see if there might be some substates hidden by averaging, but we did not find anything interesting, sharply contrasting recent reference simulations on B-DNA with complex ε/ζ BI/BII dynamics, eventually γ-trans substates.[106] This greatly simplifies all the analyses. Comparison of 50 and 500-ns trajectory portions indicates satisfactory basic convergence of the results after 50-ns (Figure 2).

dx.doi.org/10.1021/jp3014817 | J. Phys. Chem. B 2012, 116, 9899−9916

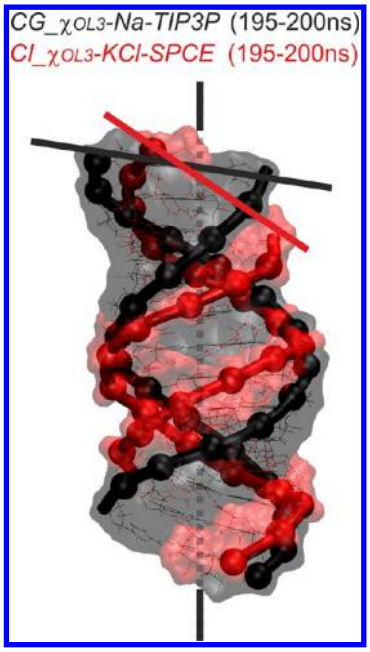

Figure 4. Comparison of geometries with maximal and minimal inclination/roll values within 10 different tracts, i.e., in black CG-tract (NN simulation, 195−200-ns averaged structure, inclination/roll values 9.9°/5.3°) and in red CI-tract (ESC0.12 simulation, 195−200-ns averaged structure, inclination/roll values 24.1°/13.4°). The black and red lines represent the inclination of one base pair with respect to the helical axes (black dashed line).

It should be noted that the simulation force field may slightly rigidify the A-RNA, as with the bsc0 correction the α/γ t/t substates are entirely eradicated (see also ref 68). Without using the bsc0 correction, the α/γ t/t substates would be present with ∼10−15% population. These α/γ t/t substates are to a certain extent seen in the X-ray structures, although many of them could be invoked by various crystal packing interactions.[56,68] Thus we suggest that the bsc0 correction makes A-RNA simulation closer to reality, in addition, the bsc0 correction visibly improves the behavior of some noncanonical RNAs, when applied together with the essential χ_{OL3} correction.[78,79]

Comparing the relative change of the structural parameters in all studied duplexes, the CG-tract is the most sensitive to change of the water/salt environment (Figure 3 and Table 2). At NN conditions, it is the "least A-form" duplex, i.e., it has the smallest inclination/roll. When simulated under ESC, its inclination/roll increase significantly, shifting the duplex deeply into the A-RNA territory. As will be explained below, the behavior mostly reflects the type of the water model.

The A-RNA Sequence Dependence Is Driven by the Shape of the WC Base Pairs. Since its discovery, it is widely assumed that a substantial part of the sequence-dependent local conformational variability of DNA and RNA double helices can be attributed to base stacking.[107] There are two main features of base stacking that can influence the double helix architecture, namely, van der Waals and electrostatic interactions. Both energy contributions are rather well described by the presently used simulation force field[32] and should thus be realistically included in the simulations, although we have recently shown that the isotropic Lennard-Jones force fields overestimate the van der Waals part of base stacking.[108]

Intrinsically (in vacuo), the electrostatic term has a larger effect on mutual orientation of stacked nucleic acids bases. However, the electrostatic contribution tends to be compensated by solvent screening in water environment. Upon full hydration, the electrostatic part of base stacking looks entirely counterbalanced by solvent screening.[109] The exact amount of solvent screening in nucleic acids is not known, and likely varies from system to system.[110] While it is possible to calculate the effect of solvent screening on free energies of nucleobase stacking in water,[109] contemporary computational chemistry, in our opinion, does not offer any reliable methodology that would allow one to quantify free energy of stacking inside different types of nucleic acids architectures.[111] The van der Waals term provides the dispersion stabilization and also determines the steric shape of the base pairs. For example, the exocyclic groups of nucleobases can significantly modulate the potential energy surface of the base pair steps, as they can lead to steric contacts upon propeller twisting.[112,113]

The electrostatic and van der Waals effects were probed by the use of the modified nucleobases, i.e., inosine (I) and 2,6-diaminopurine (D). The I−C WC base pair is a steric mimic of the A−U WC base pair, while the D−U base pair is a steric mimic of the G−C base pair, when considering the number and positions of H-bonds and exocyclic groups in the minor and major grooves (Figure 5). However, when considering molecular dipoles and electrostatics, the I−C base pair is rather similar to the G−C base pair, and the D−U pair I similar to the A−U pair[82] (Figure 6). Thus, the simulation behavior can give us a clear idea whether the electrostatic or van der

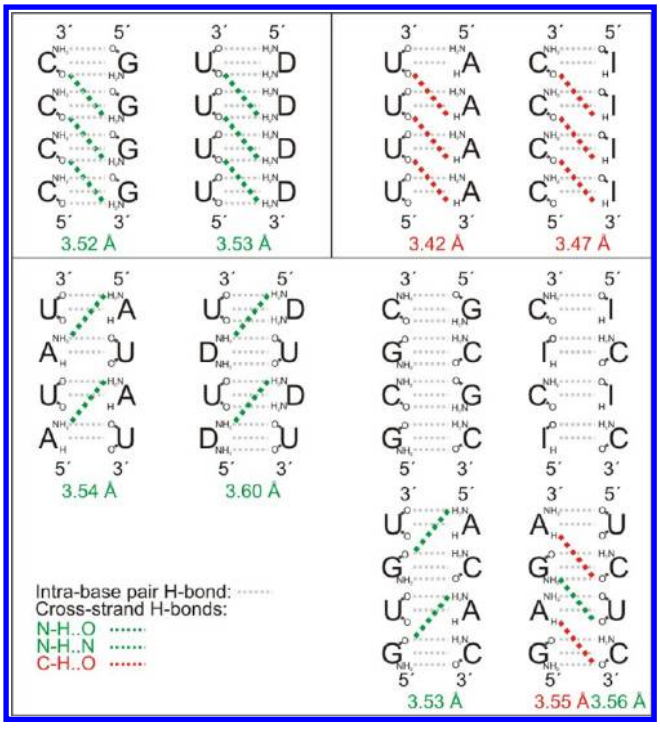

Figure 5. The scheme of base pairing and potential exocyclic cross-strand H-bonds and contacts (including adenine C2) between bases of opposite strands in the successive base pairs. We marked only those cross-strand interactions with the average length between N (or C2)...O and N...N atoms (given in red and green color, respectively) below 3.6 Å in simulations. Purely steric clashes (such as interactions of aminogroups with nucleobase rings) were not monitored. Taking into account the variation of purines/pyrimidines, number and type of H-bonds, similar sequences are grouped, mainly $(G)_{14}$ and $(D)_{14}$ and $(A)_{14}$ and $(I)_{14}$.

dx.doi.org/10.1021/jp3014817 | J. Phys. Chem. B 2012, 116, 9899−9916

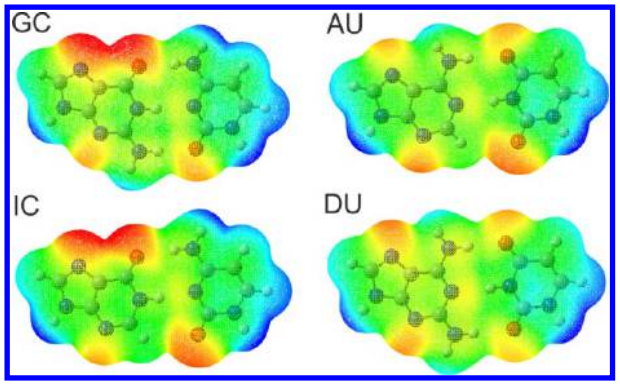

Figure 6. Electron density surface (isovalue = 0.001 au) visualized according to the value of the electrostatic potential for CG, AU, IC and DU base pairs. Note also the steric shapes. Structures were optimized in Gaussian09 by using HF/6-31*. Scale: Red ≤ −8.000e-2 au, Blue ≥ 8.000e-2 au. We used the GaussView 3.07 program for visualization.

Waals/steric properties of the base pairs dominate the sequence dependence of local variations and their solvent/ionic sensitivity.

While the oligopurine GA- and purine−pyrimidine GU-tracts are unique, for the remaining eight duplexes, we can identify pairs with similar electrostatic or shape properties. Among the oligopurine tracts, G-tract and A-tract have stericity similar to that of D-tract and I-tract, respectively (Figure 5). Their relation is interchanged when considering the electrostatics (Figure 6). The simulations clearly show that G-tract behaves similarly to D-tract, while A-tract is rather similar to I-tract (Figure 3). Thus the A-RNA compactness (inclination) reflects the stericity (shape) of the base pairs. When considering the alternating YR-tracts, CI-tract shares steric similarity with AU-tract and indeed both behave similarly considering most parameters. Further, when considering the roll/inclination graph, there is at least some resemblance between DU and CG-tracts (Figure 3), which also alternate base pairs with similar shapes. Thus, the simulations suggest that the most important factor that affects the fine shape of the 10 A-RNA duplexes (including the response to the solvent/salt change) is the van der Waals part of the stacking, i.e., the shape of the stacked base pairs, with dramatic effect of the purine minor groove exocyclic group. The A-RNA inclination variability is definitely not driven by the electrostatic contribution of stacking and exocyclic group in the major groove. Our results are consistent with an earlier study on B-DNA oligopurine tracts[85] and in fact support or resemble the decades-old suggestions by Dickerson[113] and Calladine[112] about the role of simple steric effects in determining the fine NA duplex variability.

For the sake of completeness, beside the influence of the steric shape of the nucleotides, it is also possible that the sequence dependence of the canonical A-form helix is affected by specific hydration of the minor groove.[114−117] This possibility is also consistent with the fact that duplexes with similar helical structure, e.g., G-tract and D-tract, have an identical hydrogen bonding pattern in their minor groove and, thus, presumably similar specific solvation of their minor grooves. We can not rule out that the observed dependence of A-RNA helical structure on the choice of the water model (see below) is caused by sensitivity of roll and inclination to specific solvation. Nevertheless, unambiguous separation of the steric and hydration effects, which in addition may be coupled, is not straightforward and beyond the scope of this study. We will try to resolve this issue in the near future, although trying to decompose the simulation behavior into the role of individual contributions is always risky and may lead to overinterpretation of the data.

The structures of alternating purine/pyrimidine $(RY)_7$ duplexes tended to have narrower major groove compared to R-tracts (Figure 3). We also observed the trend of higher helical twist and propeller twist values for these duplexes (Figure 3). The simulations reproduced very clearly the alternating variation of base pair roll in alternating RY helices[75,76] (see Supporting Information II).

Choice of the Water Molecules and Ions Parameters. As noted above, salt/water conditions affect the compactness of the A-RNA structure. However, the data above do not show whether the effect is due to ion type, salt concentration, or water model. Common assumption is that the compactness of A-RNA may be sensitive to the salt-strength. However, recent studies indicated that the water model may have a visible impact on the sampled solute structures and dynamics in protein and RNA simulations.[60,61,118] To separate the impact of the water model, ionic strength, and type of counterions, we conducted 50-ns MD simulations by all possible cross-settings of solvent parameters (TIP3P or SPC/E) and ions (Na^+ or K^+) under NN or ESC conditions for the CG-tract with Cheatham's ion parameters (Table 1). We have selected the $(CG)_7$ system for this investigation since this duplex was the most sensitive to the environment in the first round of computations.

The left part of Figure 7 shows by the arrows the effect of the choice of water model (TIP3P→SPC/E) on key A-RNA features under four different ion conditions. The SPC/E model leads to a visibly more compact A-RNA molecule. For example, when comparing the *CG_χ$_{OL3}$-Na-TIP3P* (50-ns) and *CG_χ$_{OL3}$-Na-SPCE* (50-ns) simulations, the major groove P...P distance for TIP3P simulation was 15.9 Å, while for SPC/E it was 12.7 Å. Use of SPC/E waters instead of TIP3P caused shift of the helical twist value from 29.7° to 30.7° (Table 3 and Figure 7). This has also been accompanied with increase of roll, slide, inclination and propeller twist by 2.7°, 0.2 Å, 4.5°, and 5°, respectively (Table 3 and Figure 7). The helical rise decreased by 0.3 Å. In general, structures simulated with SPC/E solvent were more compact compared to the equivalent TIP3P simulations (Table 3 and Figure 7).

The right part of Figure 7 shows the effect of the ion concentration (~0.18 M M^+ net-neutralization (NN) vs ~0.3 M M^+/ ~0.12 M Cl^- excess salt, i.e., ESC0.12). In general, the change of salt concentration has a rather small effect on the A-RNA geometry. Finally, when comparing the adjacent arrows in Figure 7, one can also see differences between Na^+ and K^+ ions, for different combinations of the other conditions. The potassium ions tend to support more compact A-RNA helix compared to sodium; however, the effect of ion type is significantly smaller than the water model effect.

Recent study revealed some exaggerated phosphofilicity of cations when using the Cheatham's cation parameters employed in our study.[6] Thus, we performed an additional nine 200-ns simulations of CG-tract under different KCl/TIP3P conditions, and three different sets of ion parameters (Cheatham et al.,[94] Jorgensen et al.[95] and Roux et al.[96]) were compared. In addition, we extended two earlier simulations with Cheatham's parameters to 200-ns. The results are summarized in Table 4 and Figures 8 and 9. In general, increase in the ion concentration made the $(CG)_7$ duplexes more compact. However, even when comparing the cation

dx.doi.org/10.1021/jp3014817 | J. Phys. Chem. B 2012, 116, 9899−9916

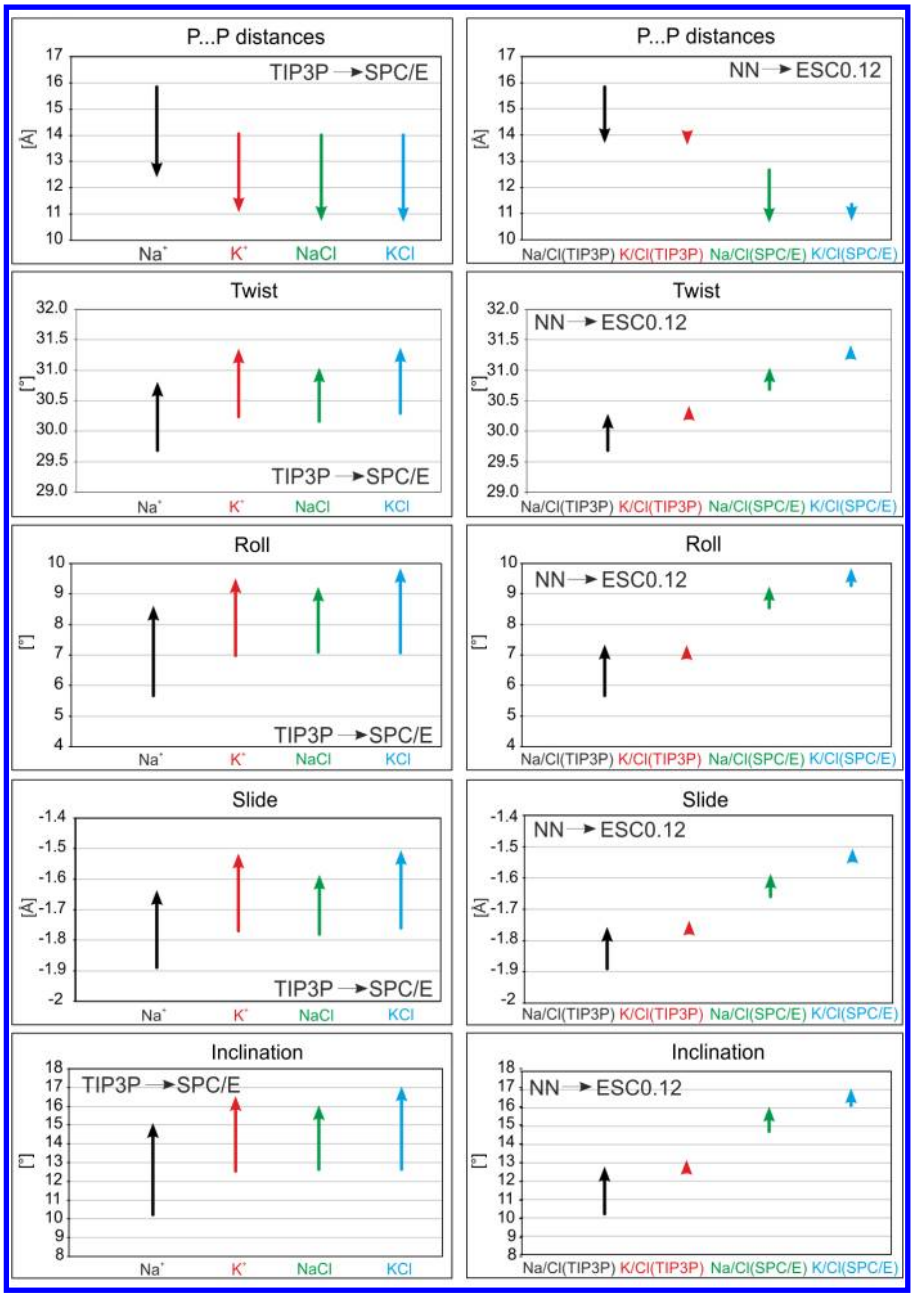

Figure 7. Impact of the water model and salt strength on selected mean structural parameters in a $(CG)_7$ RNA duplex. (Left) Each arrow represents one of the used ion concentrations (i.e., NN using either Na^+ or K^+ and ESC0.12 using either NaCl or KCl, Table 1) while the type of the water molecules changes. The arrows point from the TIP3P to the SPC/E model. (Right) Each arrow depicts the effect of two different ion strengths by using one of the cation types and water models, e.g., Na^+ (neutralized 0.18 M, NN) and NaCl (excess salt 0.3 M Na^+/0.12 M Cl^-, ESC0.12) with TIP3P, labeled as Na/Cl(TIP3P). The arrows point from NN to ESC0.12. This Figure is based on 50-ns runs. The same figure with error bars is shown in Supporting Information I, Figure S3.

concentrations in the range 0.18−1.0 M (for Cheatham's parameters), the salt effect is smaller than the effect of water model depicted in Figure 7, left. The results for the Cheatham and Roux parameters were similar (Table 4, Figures 8 and 9), while the simulations with Jorgensen ion parameters shifted the duplexes to "less compact" or inclined A-form (Table 4 and Figures 8 and 9) compared to the other two ion parameters. When comparing Cheatham and Roux ions parameters to the Jorgensen ones, the Jorgensen ions have larger radii, and their well depth is accordingly shallower. This probably causes the difference seen in the simulations, and we plan to investigate this issue in more detail in the future.

The differences of mean structural parameters revealed that the change of salt strength and type of water molecules had a nonadditive effect on sampled geometries of the duplexes. Therefore, we were not able to fully separate the influence of different ions, ionic conditions, and solvent parameters. However, comparing all the data, we conclude that the impact of the solvent type on the helical topology is larger than when varying ions and their concentrations. In conclusion, we suggest that upon changing the environment, the water model plays the most crucial role, followed in our particular case by the modest effect of choice of cation type and the even smaller effect of ion concentration. We would like to reiterate that all the

dx.doi.org/10.1021/jp3014817 | J. Phys. Chem. B 2012, 116, 9899−9916

Table 3. Summary of the Mean Structural Parameters in CG-Tracts under Different Ion/Water Conditions[a]

		Na^+ TIP3P	Na^+ SPC/E	K^+ TIP3P	K^+ SPC/E
NN	twist [°]	29.7	30.7	30.3	31.2
	roll [°]	5.7	8.4	7.1	9.3
	slide [Å]	−1.89	−1.66	−1.76	−1.54
	inclination [°]	10.2	14.7	12.6	16.1
	P...P [Å]	15.9	12.7	14.1	11.3
		NaCl TIP3P	NaCl SPC/E	KCl TIP3P	KCl SPC/E
ESC0.12	twist [°]	30.2	30.9	30.2	31.3
	roll [°]	7.1	9.0	7.0	9.6
	slide [Å]	−1.78	−1.61	−1.77	−1.53
	inclination [°]	12.6	15.7	12.6	16.7
	P...P [Å]	14.0	11.7	14.0	11.0

[a]The graphical representation of the listed values is shown in Figure 7. Estimation of errors is given in Table S4 and shown in Figure S3 in Supporting Information I.

computations were intentionally carried out for the $(CG)_7$ duplex, which shows the largest sensitivity to the changes of water/ion environment. Thus, for most other sequences, the sensitivity of the fine A-RNA structure to the environment is expected to be considerably smaller. Although we show that the results are sensitive to the water model to a certain extent, we do not want to make any suggestion as to which of the two water models is better. We consider them of comparable quality, and they are also based on the same basic approximations. We suggest that uncertainty in experimental data discussed above does not allow us to confidently suggest which of these two models is more realistic in RNA simulations.

In Supporting Information I, we provide rather extensive analysis of root-mean-square deviation (RMSd), its standard deviation, and B-factors of the studied systems. The mean RMSd and its standard deviation (describing the range of fluctuation/flexibility rather than the accuracy of the mean RMSd) for all 10 tracts was in the range of 1.2−1.7 Å (±0.25−0.45 Å), while the mean values of B-factors correlated with RMSd and varied within 26.8−40.9 $Å^2$ (Table S7 in Supporting Information I). The comparison of all three indicators also suggests that there is no substantial dependence of dynamics or flexibility on different ion parameters in MD simulations of canonical A-RNA under the studied ionic conditions (Table S7 in Supporting Information I).

Comparison with X-ray Data. In our previous study, we compared NN and ESC0.12 solution simulations with *ff*99 and *ff*99bsc0 force fields with several A-RNA X-ray structures.[68] Although different force fields and ion/water conditions provided moderately different results, we were not able to unambiguously recommend which force field and salt condition is more appropriate, because the available experimental structures show A-RNA duplexes with a wide range of compactness (inclination/roll and groove width). Since the RNA force field has been in the meantime substantially modified to the *ff*99bsc0χ_{OL3} version, we have carried out some additional comparisons of solution simulations with X-ray structures. For comparison, we used two experimental duplexes with high-resolution (1.3 and 1.55 Å, see Methods). In addition, the alternating AU-tract was compared with 1RNA X-ray structure, which shows a similar r(U(UA)$_6$A) canonical duplex at 2.25 Å resolution.[119] However, the experimental helical parameters show some irregularities and high fluctuations in structural parameters for the individual base pairs (Table S8A−C and Figure S5A−C in Supporting Information I) that might be caused by crystal packing. Thus, it is virtually impossible to propose the exact target values for comparison with the simulated structures, and the experimental data provide only approximate expected ranges of values. To smooth the irregularities in crystallographic data, we calculated mean structural parameters of the X-ray structures and compared them to solution MD values (Tables 5 and 6). The direct comparison of the variation of key helical parameters along the sequence in MD and crystal structures is shown in Supporting Information I (Table S8A−C and Figure S5A−C). The mean experimental roll/inclination values are 6.7°/12.3° for 2R20, 8.1°/15.2° for 1QC0, and 10°/18.8° for 1RNA. The simulations were performed with the most recent RNA force field *ff*99bsc0χ_{OL3}.[78,79] For the sake of completeness, we also tested two alternative χ profiles, χ_{Yil}[98] and χ_{Ode}.[99] The balance of the glycosidic angle is crucial for A-RNA helices, as they are sensitive to the orientation of nucleobases. Overpopulation of the high-*anti* region converts the A-RNA into the undesired ladder-like topology,[78] while too vigorous prevention of the high-*anti* region tends to reduce base pair inclination and roll, i.e., makes the duplex less compact and less A-form like.[78,79]

The basic results are summarized in Tables 5 and 6. The simulations confirm the general trend of the Cornell et al. force field variants to slightly underestimate helical twist. As noted above, due to uncertainty in experimental data, it is not possible to exactly determine the target values of the individual A-RNA parameters. Nevertheless, the simulations more or less agree with the experimental structures. The χ_{OL3}, χ_{Yil}, and χ_{Ode} parameters differ in the slope of the *anti* to high-*anti* region.[78,79] The χ_{OL3} parameters are optimally suited to eliminate the high-*anti* ladder-like structures while not limiting the roll/inclination

Table 4. Summary of the Mean Structural Parameters in Simulated CG-Tracts under Different Ion Strengths (K^+/KCl) and Ion Set Parameters with the TIP3P Water Model[a]

ion type	Cheatham	Jorgensen	Roux	Cheatham	Jorgensen	Roux	Cheatham	Cheatham	Jorgensen	Roux	Cheatham
salt strength	NN	NN	NN	ESC0.12	ESC0.12	ESC0.12	ESC0.32	ESC0.52	ESC0.52	ESC0.52	ESC0.82
twist [Å]	30.3	29.1	30.1	30.5	29.4	30.2	30.5	30.8	29.7	30.7	30.9
roll [°]	6.9	4.5	6.5	7.5	5.1	6.9	8.2	8.4	5.7	7.9	8.5
slide [Å]	−1.75	−1.98	−1.8	−1.72	−1.95	−1.78	−1.65	−1.65	−1.89	−1.69	−1.65
inclination [°]	12.4	8.2	11.8	13.4	9.3	12.3	14.7	14.9	10.5	14.0	14.9
h-rise [Å]	2.82	3.02	2.85	2.77	2.98	2.82	2.71	2.69	2.91	2.75	2.66
propeller [°]	−10.6	−7.0	−9.9	−11.1	−7.8	−10.3	−12.1	−12.5	−8.7	−11.7	−12.7
P...P [Å]	14.0	17.2	14.8	14.0	16.5	14.0	12.9	12.0	15.6	12.8	11.3

[a]The estimated errors of mean values are shown in Table S5 in Supporting Information I.

dx.doi.org/10.1021/jp3014817 | J. Phys. Chem. B 2012, 116, 9899−9916

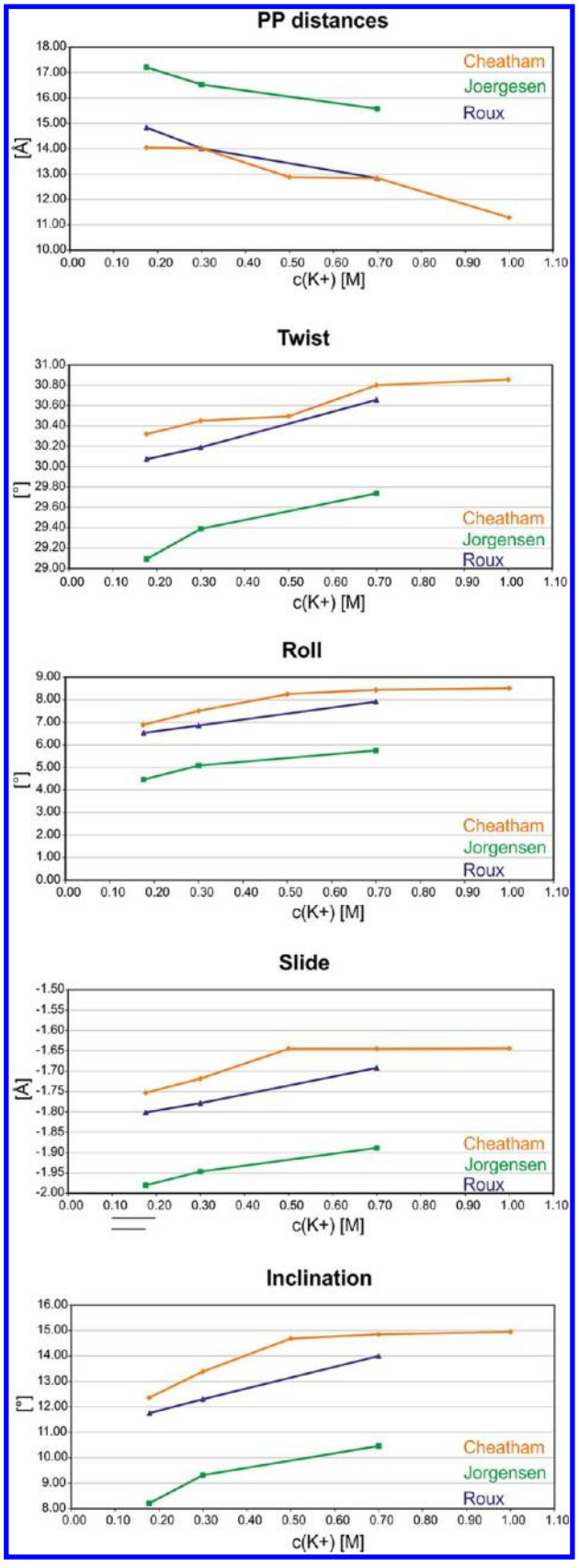

Figure 8. Impact of the ion parameter sets (Cheatham et al.,[94] Joergensen et al.,[95] and Roux et al.[96]) on the geometry of the CG-tract under different salt strengths. This figure is based on 200-ns runs.

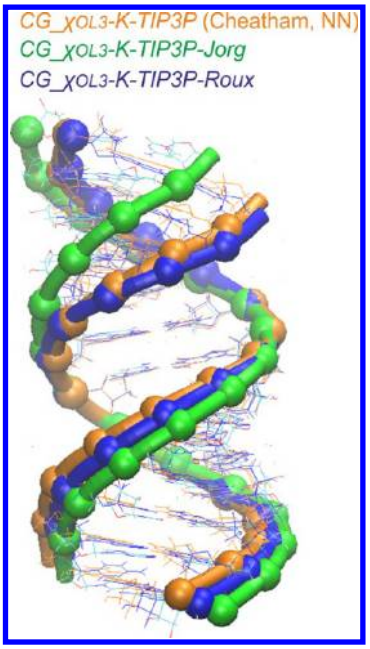

Figure 9. Comparison of average structures (45−50-ns) in net-neutralized MD simulations by using different ions parameter sets (Cheatham - orange; Jorgensen - green; Roux - blue).

of the A-RNA. The χ_{Yil} parameters to our opinion overpenalize the high-*anti* region. Thus, χ_{Yil} gives systematically lower inclination/roll (and larger P...P distances) than χ_{OL3}. It is visible especially if the original recommendation to combine χ_{Yil} with *ff*99 is followed. Then the inclination, using common Na^+/TIP3P simulation condition, is as low as 5.7° for the 1QC0 solution simulation, which is already outside the range of A-RNA experimental values. The χ_{Yil} performance is improved when combined with *ff*99bsc0 and using ESC0.12 with SPC/E. The remaining χ_{Ode} parametrization in fact promotes the high-*anti* region compared to *ff*99 (or *ff*99bsc0). This allows the simulations to sample A-RNA geometries with very high base pair inclination. However, χ_{Ode} cannot be used for RNA because it causes fast degradation to the ladder-like structure. We reiterate that the significance of the comparisons with experiments in Tables 5 and 6 should not be overrated, due to the lack of really unambiguous experimental benchmarks, as explained above. Nevertheless, our results on R-tracts seem to be consistent with the 16.4° inclination recently reported for purely canonical 16-nt RNA duplex r(AGAGAAGAUCUUCUCU) although exact comparison is again hampered by the crystal-packing related kinks affecting the experimental structure, associated with inner-shell Mg^{2+} binding accompanied with the α/γ t/t backbone substate.[120]

For the sake of completeness, a recent NMR experiment suggested an alternative A′-RNA helix characterized by ∼35.2° twist, ∼6.4° roll, ca. −1.0 Å slide, ∼3.5 Å H-rise, ∼10.1° inclination, and ca. −4.3° propeller for the longest canonical part of the structure with the sequence r(UUAUUAA).[121] The present simulations do not show any sign of the formation of such A′-RNA structure. Both A- and AU-tracts in simulations show very large inclination. In the absence of further experimental and computational data, it is not possible to decide whether this difference is due to limitations of the force field or limitations of the NMR refinement protocol. For earlier database analysis of variability of A-RNA duplexes, see ref 47.

dx.doi.org/10.1021/jp3014817 | J. Phys. Chem. B 2012, 116, 9899−9916

Table 5. The Mean Structural Parameters Averaged over 50-ns Solution Simulations of 2R20 Structures and Their Crystallographic Values

	X-ray	2R20_ff99-Na-TIP3P (NN)	2R20_ff99-KCl-SPCE (ESC0.12)	2R20_bsc0-Na-TIP3P (NN)	2R20_bsc0-KCl-SPCE (ESC0.12)	2R20_ff99-Na-TIP3P-χ_{Od} (NN)	2R20_bsc0-Na-TIP3P-χ_{Od} (NN)	2R20_χ_{OL3}-Na-TIP3P (NN)	2R20_χ_{OL3}-KCl-SPCE (ESC0.12)	2R20_ff99-Na-TIP3P-χ_{Yil} (NN)	2R20_ff99-KCl-SPCE-χ_{Yil} (ESC0.12)	2R20_bsc0-KCl-SPCE-χ_{Yil} (ESC0.12)
twist [°]	**30.7**	28.9	29.2	28.8	29.1	28.2	28.4	28.9	29.2	29.1	29.2	29.2
roll [°]	**6.7**	6.6	8.3	7.6	9.0	11.3	10.3	7.3	8.7	4.4	5.4	6.5
slide [Å]	**-1.85**	−1.74	−1.66	−1.64	−1.56	−1.16	−1.32	−1.65	−1.59	−2.10	−2.02	−1.87
inclination [°]	**12.3**	12.7	15.6	14.6	16.9	21.0	19.2	13.8	16.3	8.5	10.3	12.2
P...P [Å]	**9.5**	15.0	11.7	13.0	10.7	14.8	12.3	12.2	10.9	16.0	13.5	12.0

We also compared the atomic B-factors calculated in the solution MD simulations of 1QC0 and 2R20 structures to the X-ray data (Supporting Information IV). The B-factors from MD simulations were similar, but they differed from the X-ray values (~10 Å^2 and ~40 Å^2 for 2R20 and 1QC0, respectively). The experimental B-factors in the 1QC0 structure are systematically higher by ~30 Å^2 compared to the 2R20 data, which means that even analysis of experimental B-factors is not easy. Additionally, the MD B-factors in the two terminal nucleotides differed from X-ray values by ~200 Å^2 due to the increased flexibility of terminal base pairs that is common for RNA molecules in the solution simulations. Due to all these differences, we decided to not to attempt any interpretation of the comparison of B-factors obtained in X-ray structures and MD simulations.

The Convergence of Structural Parameters and Stability of Simulations. Convergence in simulations of nucleic acids is a complex issue. Different simulated nucleic acids systems achieve convergence of structural parameters at very different time scales. Canonical A-RNA duplexes can sample the A-RNA conformational space (from low-inclination to high-inclination) most likely without any barrier. As explained above, there do not seem to be any complex backbone substates resembling, for example, the BI/BII dynamics in B-DNA,[48,50,106] provided that the bsc0 correction is used to suppress the γ-trans states.[68]

In order to illustrate the convergence of the A-RNA simulations, we have done two simulations of $(CG)_7$ RNA duplexes starting from the canonical B-DNA geometry (simulations *BRNA_χ_{OL3}-Na-TIP3P* and *BRNA_χ_{OL3}-KCl-SPCE*). The transition from the B-RNA conformation to the A-RNA conformation occurred spontaneously within the first ~5−10-ns of the MD simulations. The overall helical parameters converged swiftly (within ~1 ns) to values typical for equivalent simulations starting from the A-RNA structure (cf. comparison with mean structural parameters in equivalent A-RNA *CG_χ_{OL3}-Na-TIP3P* and *CG_χ_{OL3}-KCl-SPCE* simulations in Figures S6−7 in Supporting Information I). The repuckering to C3′-endo was completed for all residues within 5 ns (Figure S7 in the Supporting Information). Note that visits to C3′endo pucker are rather common at the terminal base pairs and to a certain extent also in the preceding base pairs (not shown), but in general do not occur in the 10 internal base pairs considered for our analyses. For the sake of completeness, we acknowledge some earlier studies that investigated the B to A transitions in canonical nucleic acids duplexes.[8,122,123] Even faster convergence to the expected geometry was achieved in "cross-condition" simulations of the CG-tract performed under NN (*CG(ESC0.12)_χ_{OL3}-Na-TIP3P*) and ESC0.12 (*CG(NN)_χ_{OL3}-KCl-SPCE*) conditions, where the starting structure had geometry from the end of the *CG_χ_{OL3}-Na-TIP3P* (ESC0.12) and *CG_χ_{OL3}-KCl-SPCE* (NN) simulations, respectively (Figure S8 in Supporting Information I). Thus, all our data suggest that simulated canonical A-RNA can rather quickly shake off details of the starting structure and achieve converged distribution of parameters on ~10−50-ns time scale, even when starting from B-RNA conformation. A-RNA simulations smoothly sample the A-RNA conformational space, which lacks any substantial barriers that would lock the molecules in some long-living substates. The simulations quickly find the optimal geometry for a given sequence, force field, and ion/water conditions, irrespective of the starting structure. This is fully supported by the set of 200-ns-long trajectories discussed

dx.doi.org/10.1021/jp3014817 | J. Phys. Chem. B 2012, 116, 9899−9916

Table 6. Selected Mean Structural Parameters over 50-ns for the 1QC0 Solution Simulations

	X-ray	*1QC0_ff99-Na-TIP3P-χ_{Ode}* (NN)	*1QC0_χ_{OL3}-Na-TIP3P* (NN)	*1QC0_χ_{OL3}-KCl-SPCE* (ESC0.12)	*1QC0_ff99-Na-TIP3P-χ_{Yil}* (NN)	*1QC0_ff99-KCl-SPCE-χ_{Yil}* (ESC0.12)	*1QC0_bsc0-KCl-SPCE-χ_{Yil}* (ESC0.12)
twist [°]	**30.8**	28.2	28.9	30.3	27.4	29.1	29.3
roll [°]	**8.1**	7.7	7.4	9.7	3.0	5.5	6.5
slide [Å]	**-1.70**	−1.94	−1.85	−1.57	−2.35	−2.07	−1.91
inclination [°]	**15.2**	14.7	13.9	17.7	5.7	10.4	12.0
P...P [Å]	**11.6**	16.6	13.7	10.1	16.8	15.0	13.3

above; their first 50-ns portions were fully representative in all cases. We obviously do not convey that the 50 and 200-ns simulations provide entirely identical results. However, there are no systematic differences and no differences that would be of any significance. All basic results of the present paper could be achieved with just 50-ns time scale.

Further, we analyzed the convergence issue using 500-ns-long simulations of $(CG)_7$ sequences (*CG_χ_{OL3}-Na-TIP3P* and *CG_χ_{OL3}-KCl-SPCE*). Table S9A,B in Supporting Information I shows the mean helical parameters averaged over the individual 10-ns windows. We further analyzed the date according to two standard procedures:[106,124] (i) The mean structural parameters were computed and validated on the halves of both 500-ns-long trajectories separately and afterward compared with the mean values from the initial 50-ns (Table S10 in Supporting Information I). The mean structural parameters for both halves were consistent with the average values from each 500-ns-long simulation as well as from the initial 50-ns-long part. Overlay of geometries from the ends of 50-ns- and 500-ns-long simulations are shown in Figure 2, and the mean structural parameters are compared in Table 7 for both intervals. (ii) Further, the structures were split into two blocks with base pairs 3−7 and 8−12 (Table S11 in Supporting Information I). Comparing mean structural parameters from both blocks resulted in very good agreement. The differences of average parameters between both blocks did not reach 0.03 Å and 0.2° for the 500-ns trajectory. All the data together suggest that for canonical A-RNA double helices, 50-ns time scale is fairly sufficient to achieve satisfactory convergence of the A-RNA structures derived from MD simulations. We again reiterate that we do not suggest that there are no fluctuations in the simulations. For example, in the 10-ns windows of the 500-ns CG-tract simulations, the mean helix inclination varies from 7.0° to 11.6° in the NN Na^+ TIP3P simulation and from 14.6° to 17.9° in the ESC0.12 KCl SPC/E simulation (Supporting Information, Table S9A,B). However, averaging over the 200-ns simulations used for most of our analyses should provide already a very stable picture of the parameters (Supporting Information, Table S3).

We have also carried out the Man−Kendall test.[104] The hypothesis that there is no trend in the helical parameters in the simulations was above 50% for all 200-ns tract simulations (for more information, see Supporting Information I, Figures S9−10 and Table S12)

The two 0.5 μs simulations of the CG-tract maintained compact helical shape. The disruption of one terminal base pair appeared in the *CG_χ_{OL3}-Na-TIP3P* (NN) and *CG_χ_{OL3}-KCl-SPCE* (ESC0.12) simulations after 163 and 58 ns, respectively. One of the terminal bases flipped out and moved freely, while the second one stayed fixed by stacking interactions in the original base pair position. The force field was able to repair and reform the original canonical CG base pair within next 155 ns in the *CG_χ_{OL3}-Na-TIP3P* run. In the case of the *CG_χ_{OL3}-KCl-SPCE* simulation, the loss of CG base pair was irreversible on the simulation time scale.

Table 7. The Averages of the Selected Structural Parameters over Different Intervals (1−50 and 1−500-ns) in Both 500-ns-Long Trajectories of the CG Tracts[a]

	CG_χ_{OL3}-Na-TIP3P		*CG_χ_{OL3}-KCl-SPCE*	
	1−50-ns	1−500-ns	1−50-ns	1−500-ns
twist [°]	29.7	29.5	31.3	31.2
roll [°]	5.7	5.4	9.6	9.4
slide [Å]	−1.89	−1.91	−1.53	−1.53
inclination [°]	10.2	9.8	16.7	16.4

[a]See also Table S6 for errors estimation in Supporting Information I.

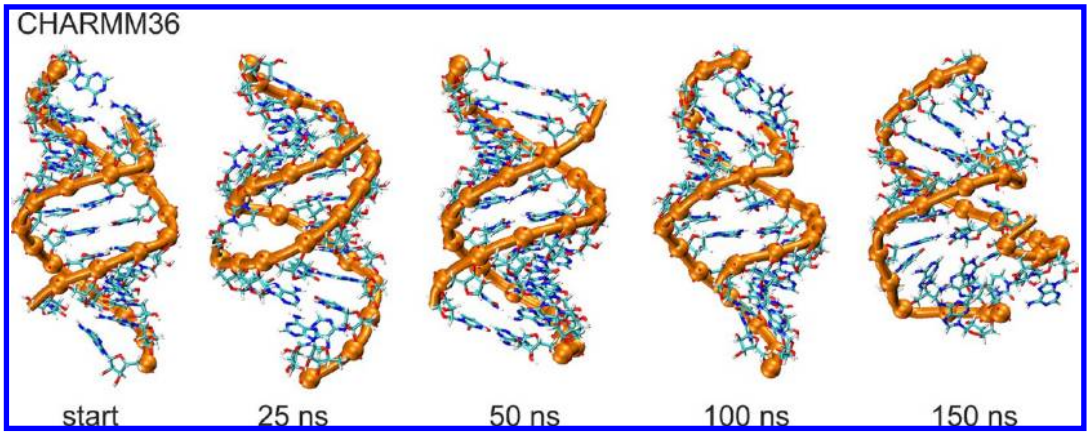

Figure 10. Development of the structure of the CG tract under excess-salt KCl (ESC0.12) conditions when using the CHARMM36 force field: starting structure and structures at 25 ns, 50-ns, 100 and 150-ns. TIP3P water model has been used.

No disruptions or long opening events of the base pairs occurred during the first 50-ns portions of the tract simulations except for broken H-bond pattern in one terminal AU pair in AU-tract after 34 ns. We did not follow the 50−200-ns portions of the 200-ns simulations in detail in this respect; however, visual inspection did not indicate any problems. However, when using the Ode et al. modification,[99] the simulated duplexes converted to the ladder-like geometry even on the 50-ns time scale (data not shown), so that this parametrization accelerates the formation of ladders as noted earlier[78] and should in no case be used for RNA simulations.

CHARMM Simulations. We also did not analyze the CHARMM simulations in detail, because they show (at least in the test that we have done), lower structural stability. For more details, see Figure 10 and Table S13, Table S14A−E, and Figures S11−16 in Supporting Information I. Some problems occurred even when using the recent reparameterization of the 2′OH dihedrals (CHARMM36).[87] The lower structural stability of A-RNA accompanied by frequent base pair opening in CHARMM27 simulations has been repeatedly reported in the literature.[78,88,125−127] The same behavior, i.e., frequent breaking of base pairs and/or formation of noncanonical WC pairs, was observed in our simulations with the CHARMM27 force field (Figure S15). A-RNA duplexes with AU pairs showed higher tendency for base pair breaking and lower structural stability than the CG A-RNA duplex. The reason for the propensity of CHARMM to opening and loss of base pair is not fully clear. Older quantum chemical literature suggested that the CHARMM27 force field may somewhat underestimate base pairing energy.[128] However, this claim has later been challenged, and the duplex instability has been attributed to incorrect torsional profile of the 2′OH group of ribose in CHARMM27. This torsion has been reparametrized accordingly, leading to the CHARMM36 version.[87] Still, even with CHARMM36, we see, albeit less frequently, instabilities due to breaking of base pairs (Figure 10), at least with our particular simulation setup. Thus we postponed further testing of the force field to future studies.

CONCLUSIONS

The calculations show that the A-RNA helix compactness, described mainly by the geometrical parameters inclination, base pair roll and helical rise, is sequence-dependent. In the calculated set of structures, the inclination varies from 10° to 24°. Using simulations with modified bases (inosine and 2,6-diaminopurine) we demonstrate that the sequence-dependence of purely canonical A-RNA double helix is caused by (or at least correlates with) the steric shape of the base pairs, i.e., the van der Waals interactions. The electrostatic part of stacking does not appear to affect the A-RNA shape. Especially visible is the role of the minor groove amino group of purines. This resembles the so-called Dickerson−Calladine mechanical rules of double helix sequence-dependent variability.[112,113] We did not identify any long-living backbone substate in A-RNA double helices that would resemble for example the B-DNA BI/BII dynamics. The variability of the A-RNA compactness is exclusively due to mutual movements of the consecutive base pairs coupled with modest change of the glycosidic χ torsion (around 12°). The other backbone dihedrals do not change upon the change of the A-RNA compactness. The A-RNA simulations appear to be converged within 50-ns, provided the γ-trans substates are prevented by the bsc0 correction.

We found that among all tested RNA force fields (Cornell et al. types: *ff*99bsc0χ_{OL3},[71,78,79] *ff*99bsc0χ_{Yil},[71,98] *ff*99χ_{Yil},[71,98] *ff*99bsc0χ_{Ode},[71,99] *ff*99χ_{Ode},[99] and CHARMM types: CHARMM27[86] and CHARMM36[87]), the latest version with *ff*99bsc0[71] correction to α/γ torsions and χ_{OL3}[78,79] correction to glycosidic torsion provides the most consistent results. Some (albeit not all) other force fields can lead to visible instabilities, as specified above.

We analyzed the influence of solvent and ionic conditions on the helical structure of A-RNA duplexes and the sequence specificity of such sensitivity. The water model choice has the most visible effect on the helical structure of A-form duplexes. A considerably smaller effect comes from the types of ions and different ionic strengths. The water model dependency is sequence-dependent with the most sensitive sequence being the $(CG)_7$ duplex with alternating CG and GC base pairs.

ASSOCIATED CONTENT

Supporting Information

Part I: (1) The AMBER prep-files of I and D nucleotides; (2) list of P...P distances in all studied helices (Table S1); (3) chosen mean structural parameters over the first 50-ns of all tract simulations (Table S2 and Figure S1); (4) selected mean structural parameters (and their correlations) with error bars for different sequences calculated for all simulated R- and YR-tracts by applying different salt conditions and solvent models (NN with TIP3P and ESC0.12 with SPC/E) (Table S3 and Figure S2); (5) impact of the water model (TIP3P and SPC/E) and salt strength (NN-Na+/K+, ESC-NaCl/KCl) on selected mean structural parameters in $r(CG)_7$ RNA duplex (Table S4 and Figure S3); (6) overlay of AU- and CG-tract under NN condition (Figure S4); (7) summary of the mean structural parameters with estimated errors in CG-tracts under different ion strength (K^+/KCl) and three different ions set parameters with TIP3P water model (Table S5); (9) the averages of the selected structural parameters and estimation of their errors over different intervals (1 − 50 and 1 − 500-ns) in both 500-ns-long trajectories of the CG tracts (Table S6); (10) average RMSd, its standard deviations, and B-factors of nucleotides for all 10 studied tracts (Table S7); (11) comparison of base pair and base pair step parameters of double helical 2R20 and 1QC0 structures in X-ray data and MD simulations (Table S8A−C, Figure S5A−C); (12) time development of averaged structural parameters in simulations *BRNA_*χ_{OL3}*-Na-TIP3P* and *BRNA_*χ_{OL3}*-KCl-SPCE* (Figure S6, Figure S7); (13) time development of averaged structural parameters in simulations *CG(ESC0.12)_*χ_{OL3}*-Na-TIP3P* and *CG(NN)_*χ_{OL3}*-KCl-SPCE* (Figure S8); (14) time development of mean structural parameters in the 0.5 μs simulations of CG-tracts (Tables S10 A-B); (15) table of mean structural parameters over 1−250-ns, 251−500 and 50-ns-long parts of 0.5 μs simulations of CG-tracts (Table S11); (16) table of mean structural parameters calculated by using 3rd to 7th and 8th to 12th base pairs for 500 and 50-ns intervals of the CG-tracts simulations (Table S12); (17) estimation of decorrelation time by using autocorrelation function calculated for twist in *CG_*χ_{OL3}*-KCl-SPCE* simulation (Figures S9−10); (18) Mann−Kendall test for the 10 studied A-RNA tracts (Table S12); (19) methods for the CHARMM MD simulations; (20) overview of the CHARMM simulations (Table S13); (21) the development of selected structural parameters in the CHARMM simulations (Table S14A−E); (22) the development of $(UA)_6A$ and $(GC)_6C$ structures and their RMSd in the CHARMM simulations (Figures S11−14);

dx.doi.org/10.1021/jp3014817 | J. Phys. Chem. B 2012, 116, 9899−9916

(23) development of base pairing in all eight CHARMM simulations (Figure S16); (24) Development of RMSd in the CHARMM trajectories (Figure S16). Part II: The development of all listed base pair and base pair step parameters, sugar pucker, and glycosidic angles in 10-ns intervals for each base pair (or each nucleotide) in the course of each 200-ns-long trajectory. Part III: The development of all backbone dihedral angles in 10-ns intervals for the individual nucleotides during each 200-ns-long trajectory. Part IV: Comparison of B-factors in X-ray data and MD simulations. This material is available free of charge via the Internet at http://pubs.acs.org.

AUTHOR INFORMATION

Corresponding Author

*E-mail: sponer@ncbr.muni.cz; FAX: + 420 541 211 293; Phone: + 420 541 517 133.

Notes

The authors declare no competing financial interest.

ACKNOWLEDGMENTS

This work was supported by the Ministry of Education, Youth and Sports of the Czech Republic: Projects "CEITEC - Central European Institute of Technology" (CZ.1.05/1.1.00/02.0068) and "RCPTM - Regional Centre of Advanced Technologies and Materials" (CZ.1.05/2.1.00/03.0058) from the European Regional Development Fund, and "RCPTM-TEAM", (CZ.1.07/2.3.00/20.0017, M.O., P.B.) from the Operational Program Education for Competitiveness - European Social Fund and by the Grant Agency of the Czech Republic [203/09/1476 (J.S.), 203/09/H046 (I.B.), P208/12/1878 (M.O.), P301/11/P558 (P.B.) and P305/12/G03 (I.B., J.S.)].

REFERENCES

(1) Anderson, C. F.; Record, M. T. *Annu. Rev. Phys. Chem.* **1995**, *46*, 657−700.
(2) Rouzina, I.; Bloomfield, V. A. *Biophys. J.* **1998**, *74*, 3152−3164.
(3) Strauss, J. K.; Maher, L. J. *Science* **1994**, *266*, 1829−1834.
(4) McFail-Isom, L.; Sines, C. C.; Williams, L. D. *Curr. Opin. Struct. Biol.* **1999**, *9*, 298−304.
(5) Ng, H. L.; Dickerson, R. E. *Nucleic Acids Res.* **2002**, *30*, 4061−4067.
(6) Noy, A.; Soteras, I.; Luque, F. J.; Orozco, M. *Phys. Chem. Chem. Phys.* **2009**, *11*, 10596−10607.
(7) Draper, D. E.; Grilley, D.; Soto, A. M. *Annu. Rev. Biophys. Biomol. Struct.* **2005**, *34*, 221−243.
(8) Cheatham, T. E.; Young, M. A. *Biopolymers* **2000**, *56*, 232−256.
(9) Lane, A. N.; Chaires, J. B.; Gray, R. D.; Trent, J. O. *Nucleic Acids Res.* **2008**, *36*, 5482−5515.
(10) Leontis, N. B.; Lescoute, A.; Westhof, E. *Curr. Opin. Struct. Biol.* **2006**, *16*, 279−287.
(11) Jaeger, L.; Verzemnieks, E. J.; Geary, C. *Nucleic Acids Res.* **2009**, *37*, 215−230.
(12) Sponer, J.; Sponer, J. E.; Petrov, A. I.; Leontis, N. B. *J. Phys. Chem. B* **2010**, *114*, 15723−15741.
(13) Mergny, J. L.; De Cian, A.; Ghelab, A.; Sacca, B.; Lacroix, L. *Nucleic Acids Res.* **2005**, *33*, 81−94.
(14) Neidle, S. *Curr. Opin. Struct. Biol.* **2009**, *19*, 239−250.
(15) Auffinger, P.; Grover, N.; Westhof, E. Metal ion binding to RNA. In *Structural and Catalytic Roles of Metal Ions in RNA*; Siegel, A., Siegel, H., Siegel, R. O. K., Eds.; The Royal Society of Chemistry: Cambridge, U.K., 2011; Vol. *9*, pp 1−35.
(16) Draper, D. E. *RNA* **2004**, *10*, 335−343.
(17) Ennifar, E.; Walter, P.; Dumas, P. *Nucleic Acids Res.* **2003**, *31*, 2671−2682.
(18) Soto, A. M.; Misra, V.; Draper, D. E. *Biochemistry* **2007**, *46*, 2973−2983.
(19) Woodson, S. A. *Curr. Opin. Chem. Biol.* **2005**, *9*, 104−109.
(20) Woods, K. K.; McFail-Isom, L.; Sines, C. C.; Howerton, S. B.; Stephens, R. K.; Williams, L. D. *J. Am. Chem. Soc.* **2000**, *122*, 1546−1547.
(21) Erat, M. C.; Sigel, R. K. O. Methods to Detect and Characterize Metal Ion Binding Sites in RNA. In *Structural and Catalytic Roles of Metal Ions in RNA*; Siegel, H., Siegel, R. O. K., Eds.; The Royal Society of Chemistry: Cambridge, U.K., 2011; Vol. *9*, pp 37−100.
(22) Bowman, J. C.; Lenz, T. K.; Hud, N. V.; Williams, L. D. *Curr. Opin. Struct. Biol.* **2012**, DOI: 10.1016/j.sbi.2012.1004.1006.
(23) Auffinger, P.; Bielecki, L.; Westhof, E. *Structure* **2004**, *12*, 379−388.
(24) Spackova, N.; Berger, I.; Sponer, J. *J. Am. Chem. Soc.* **2001**, *123*, 3295−3307.
(25) Krasovska, M. V.; Sefcikova, J.; Reblova, K.; Schneider, B.; Walter, N. G.; Sponer, J. *Biophys. J.* **2006**, *91*, 626−638.
(26) Reblova, K.; Spackova, N.; Sponer, J. E.; Koca, J.; Sponer, J. *Nucleic Acids Res.* **2003**, *31*, 6942−6952.
(27) Chen, A. A.; Draper, D. E.; Pappu, R. V. *J. Mol. Biol.* **2009**, *390*, 805−819.
(28) Auffinger, P.; Bielecki, L.; Westhof, E. *J. Mol. Biol.* **2004**, *335*, 555−571.
(29) Singh, A.; Sethaphong, L.; Yingling, Y. G. *Biophys. J.* **2011**, *101*, 727−735.
(30) Fadrna, E.; Spackova, N.; Sarzynska, J.; Koca, J.; Orozco, M.; Cheatham, T. E.; Kulinski, T.; Sponer, J. *J. Chem. Theory Comput.* **2009**, *5*, 2514−2530.
(31) Reblova, K.; Sponer, J. E.; Spackova, N.; Besseova, I.; Sponer, J. *J. Phys. Chem. B* **2011**, *115*, 13897−13910.
(32) Ditzler, M. A.; Otyepka, M.; Sponer, J.; Walter, N. G. *Acc. Chem. Res.* **2010**, *43*, 40−47.
(33) Reblova, K.; Spackova, N.; Stefl, R.; Csaszar, K.; Koca, J.; Leontis, N. B.; Sponer, J. *Biophys. J.* **2003**, *84*, 3564−3582.
(34) Young, M. A.; Jayaram, B.; Beveridge, D. L. *J. Am. Chem. Soc.* **1997**, *119*, 59−69.
(35) Sgrignani, J.; Magistrato, A. *J. Phys. Chem. B* **2012**, DOI: 10.1021/jp206475d.
(36) Do, N. T.; Ippoliti, E.; Carloni, P.; Varani, G.; Parrinello, M. *J. Chem. Theory Comput.* **2012**, DOI: 10.1021/ct2005769.
(37) Rueda, M.; Cubero, E.; Laughton, C. A.; Orozco, M. *Biophys. J.* **2004**, *87*, 800−811.
(38) Perez, A.; Luque, F. J.; Orozco, M. *J. Am. Chem. Soc.* **2007**, *129*, 14739−14745.
(39) Auffinger, P.; Westhof, E. *J. Mol. Biol.* **2000**, *300*, 1113−1131.
(40) Auffinger, P.; Westhof, E. *J. Mol. Biol.* **2001**, *305*, 1057−1072.
(41) Auffinger, P.; Bielecki, L.; Westhof, E. *Chem. Biol.* **2003**, *10*, 551−561.
(42) Allner, O.; Nilsson, L.; Villa, A. *J. Chem. Theory Comput.* **2012**, *8*, 1493−1502.
(43) Auffinger, P. Ions in Molecular Dynamics Simulations of RNA Systems. In *RNA 3D Structure Analysis and Prediction*; Leontis, N. B., Westhof, E., Eds.; Springer-Verlag: Berlin, 2012; Vol. *27*, pp 299−318.
(44) Wong, K. Y.; Lee, T. S.; York, D. M. *J. Chem. Theory Comput.* **2011**, *7*, 1−3.
(45) Wheatley, E. G.; Pieniazek, S. N.; Mukerji, I.; Beveridge, D. L. *Biophys. J.* **2012**, *102*, 552−560.
(46) Kirmizialtin, S.; Elber, R. *J. Phys. Chem. B* **2010**, *114*, 8207−8220.
(47) Perez, A.; Noy, A.; Lankas, F.; Luque, F. J.; Orozco, M. *Nucleic Acids Res.* **2004**, *32*, 6144−6151.
(48) Beveridge, D. L.; Barreiro, G.; Byun, K. S.; Case, D. A.; Cheatham, T. E.; Dixit, S. B.; Giudice, E.; Lankas, F.; Lavery, R.; Maddocks, J. H.; et al. *Biophys. J.* **2004**, *87*, 3799−3813.
(49) Noy, A.; Perez, A.; Lankas, F.; Luque, F. J.; Orozco, M. *J. Mol. Biol.* **2004**, *343*, 627−638.

(50) Dixit, S. B.; Beveridge, D. L.; Case, D. A.; Cheatham, T. E.; Giudice, E.; Lankas, F.; Lavery, R.; Maddocks, J. H.; Osman, R.; Sklenar, H.; et al. *Biophys. J.* **2005**, *89*, 3721−3740.
(51) Perez, A.; Lankas, F.; Luque, F. J.; Orozco, M. *Nucleic Acids Res.* **2008**, *36*, 2379−2394.
(52) Sponer, J.; Spackova, N. *Methods* **2007**, *43*, 278−290.
(53) Schlick, T. *Molecular Modeling: An Interdisciplinary Guide*; Springer: New York, 2010; Vol. 2.
(54) McDowell, S. E.; Spackova, N.; Sponer, J.; Walter, N. G. *Biopolymers* **2007**, *85*, 169−184.
(55) Sponer, J.; Cang, X.; Cheatham, T. E., III. *Methods* **2012**, DOI: 10.1016/j.bbr.2011.1003.1031.
(56) Reblova, K.; Lankas, F.; Razga, F.; Krasovska, M. V.; Koca, J.; Sponer, J. *Biopolymers* **2006**, *82*, 504−520.
(57) Wong, V.; Case, D. A. *J. Phys. Chem. B* **2008**, *112*, 6013−6024.
(58) Shirts, M. R.; Pande, V. S. *J. Chem. Phys.* **2005**, 122.
(59) Nutt, D. R.; Smith, J. C. *J. Chem. Theory Comput.* **2007**, *3*, 1550−1560.
(60) Florova, P.; Sklenovsky, P.; Banas, P.; Otyepka, M. *J. Chem. Theory Comput.* **2010**, *6*, 3569−3579.
(61) Sklenovsky, P.; Florova, P.; Banas, P.; Reblova, K.; Lankas, F.; Otyepka, M.; Sponer, J. *J. Chem. Theory Comput.* **2011**, *7*, 2963−2980.
(62) Glass, D. C.; Krishnan, M.; Nutt, D. R.; Smith, J. C. *J. Chem. Theory Comput.* **2010**, *6*, 1390−1400.
(63) Jorgensen, W. L.; Chandrasekhar, J.; Madura, J. D.; Impey, R. W.; Klein, M. L. *J. Chem. Phys.* **1983**, *79*, 926−935.
(64) Mahoney, M. W.; Jorgensen, W. L. *J. Chem. Phys.* **2000**, *112*, 8910−8922.
(65) Mahoney, M. W.; Jorgensen, W. L. *J. Chem. Phys.* **2001**, *114*, 363−366.
(66) Berendsen, H. J. C.; Grigera, J. R.; Straatsma, T. P. *J. Phys. Chem.* **1987**, *91*, 6269−6271.
(67) Mark, P.; Nilsson, L. *J. Phys. Chem. A* **2001**, *105*, 9954−9960.
(68) Besseova, I.; Otyepka, M.; Reblova, K.; Sponer, J. *Phys. Chem. Chem. Phys.* **2009**, *11*, 10701−10711.
(69) Cornell, W. D.; Cieplak, P.; Bayly, C. I.; Gould, I. R.; Merz, K. M.; Ferguson, D. M.; Spellmeyer, D. C.; Fox, T.; Caldwell, J. W.; Kollman, P. A. *J. Am. Chem. Soc.* **1995**, *117*, 5179−5197.
(70) Wang, J. M.; Cieplak, P.; Kollman, P. A. *J. Comput. Chem.* **2000**, *21*, 1049−1074.
(71) Perez, A.; Marchan, I.; Svozil, D.; Sponer, J.; Cheatham, T. E.; Laughton, C. A.; Orozco, M. *Biophys. J.* **2007**, *92*, 3817−3829.
(72) Bhattacharyya, D.; Bansal, M. *J. Biomol. Struct. Dyn.* **1994**, *11*, 1251−1275.
(73) Bhattacharyya, D.; Bansal, M. *J. Biomol. Struct. Dyn.* **1989**, *6*, 635−653.
(74) Bhattacharyya, D.; Bansal, M. *J. Biomol. Struct. Dyn.* **1990**, *8*, 539−572.
(75) Sponer, J.; Kypr, J. *J. Mol. Biol.* **1991**, *221*, 761−764.
(76) Wahl, M. C.; Sundaralingam, M. *Biopolymers* **1997**, *44*, 45−63.
(77) Mlynsky, V.; Banas, P.; Hollas, D.; Reblova, K.; Walter, N. G.; Sponer, J.; Otyepka, M. *J. Phys. Chem. B* **2010**, *114*, 6642−6652.
(78) Banas, P.; Hollas, D.; Zgarbova, M.; Jurecka, P.; Orozco, M.; Cheatham, T. E.; Sponer, J.; Otyepka, M. *J. Chem. Theory Comput.* **2010**, *6*, 3836−3849.
(79) Zgarbova, M.; Otyepka, M.; Sponer, J.; Mladek, A.; Banas, P.; Cheatham, T. E.; Jurecka, P. *J. Chem. Theory Comput.* **2011**, *7*, 2886−2902.
(80) Tolbert, B. S.; Miyazaki, Y.; Barton, S.; Kinde, B.; Starck, P.; Singh, R.; Bax, A.; Case, D. A.; Summers, M. F. *J. Biomol. NMR* **2010**, *47*, 205−219.
(81) Sponer, J.; Jurecka, P.; Hobza, P. *J. Am. Chem. Soc.* **2004**, *126*, 10142−10151.
(82) Sponer, J.; Leszczynski, J.; Hobza, P. *J. Phys. Chem.* **1996**, *100*, 1965−1974.
(83) Bailly, C.; Waring, M. J. *Nucleic Acids Res.* **1998**, *26*, 4309−4314.
(84) Shatzky-Schwartz, M.; Arbuckle, N. D.; Eisenstein, M.; Rabinovich, D.; Bareket-Samish, A.; Haran, T. E.; Luisi, B. F.; Shakked, Z. *J. Mol. Biol.* **1997**, *267*, 595−623.
(85) Lankas, F.; Cheatham, T. E.; Spackova, N.; Hobza, P.; Langowski, J.; Sponer, J. *Biophys. J.* **2002**, *82*, 2592−2609.
(86) Foloppe, N.; MacKerell, A. D. *J. Comput. Chem.* **2000**, *21*, 86−104.
(87) Denning, E. J.; Priyakumar, U. D.; Nilsson, L.; Mackerell, A. D. *J. Comput. Chem.* **2011**, *32*, 1929−1943.
(88) Faustino, I.; Perez, A.; Orozco, M. *Biophys. J.* **2010**, *99*, 1876−1885.
(89) Case, D. A.; Darden, T. A.; Cheatham, T. E., III; Simmerling, C. L.; Wang, J.; Duke, R. E.; Luo, R.; Crowley, M.; Walker, R. C.; Zhang, W. et al. *AMBER 10.0*; University of California: San Francisco, CA, 2008.
(90) Frisch, M. J.; Trucks, G. W.; Schlegel, H. B.; Scuseria, G. E.; Robb, M. A.; Cheeseman, J. R.; Montgomery, J. J. A.; Vreven, T.; Kudin, K. N.; Burant, J. C. et al. *Gaussian 09*; Gaussian, Inc.: Wallingford, CT, 2004.
(91) Wang, J. M.; Wang, W.; Kollman, P. A.; Case, D. A. *J. Mol. Graph. Model.* **2006**, *25*, 247−260.
(92) Timsit, Y.; Bombard, S. *RNA* **2007**, *13*, 2098−2107.
(93) Klosterman, P. S.; Shah, S. A.; Steitz, T. A. *Biochemistry* **1999**, *38*, 14784−14792.
(94) Joung, I. S.; Cheatham, T. E. *J. Phys. Chem. B* **2008**, *112*, 9020−9041.
(95) Jorgensen, W. L.; Maxwell, D. S.; TiradoRives, J. *J. Am. Chem. Soc.* **1996**, *118*, 11225−11236.
(96) Roux, B. *Biophys. J.* **1996**, *71*, 3177−3185.
(97) Duke, R. E.; Pedersen, L. G. *PMEMD*; University of North Carolina-Chapel Hill: Chapel Hill, NC, 2003.
(98) Yildirim, I.; Stern, H. A.; Kennedy, S. D.; Tubbs, J. D.; Turner, D. H. *J. Chem. Theory Comput.* **2010**, *6*, 1520−1531.
(99) Ode, H.; Matsuo, Y.; Neya, S.; Hoshino, T. *J. Comput. Chem.* **2008**, *29*, 2531−2542.
(100) Darden, T.; York, D.; Pedersen, L. *J. Chem. Phys.* **1993**, *98*, 10089−10092.
(101) Essmann, U.; Perera, L.; Berkowitz, M. L.; Darden, T.; Lee, H.; Pedersen, L. G. *J. Chem. Phys.* **1995**, *103*, 8577−8593.
(102) Berendsen, H. J. C.; Postma, J. P. M.; Vangunsteren, W. F.; Dinola, A.; Haak, J. R. *J. Chem. Phys.* **1984**, *81*, 3684−3690.
(103) Lu, X. J.; Olson, W. K. *Nucleic Acids Res.* **2003**, *31*, 5108−5121.
(104) Hipel, K. W.; McLeod, A. I. *Time Series Modelling of Water Resources and Environmental System*; Elsevier: Amsterdam, 1994.
(105) Humphrey, W.; Dalke, A.; Schulten, K. *J. Mol. Graph.* **1996**, *14*, 33−38.
(106) Lavery, R.; Zakrzewska, K.; Beveridge, D.; Bishop, T. C.; Case, D. A.; Cheatham, T.; Dixit, S.; Jayaram, B.; Lankas, F.; Laughton, C.; et al. *Nucleic Acids Res.* **2010**, *38*, 299−313.
(107) Dickerson, R. E.; Drew, H. R. *J. Mol. Biol.* **1981**, *149*, 761−786.
(108) Banas, P.; Mladek, A.; Otyepka, M.; Zgarbova, M.; Jurecka, P.; Svozil, D.; Lankas, F.; Sponer, J. *J. Chem. Theory Comput.* **2012**, DOI: 10.1021/ct3001238.
(109) Florian, J.; Sponer, J.; Warshel, A. *J. Phys. Chem. B* **1999**, *103*, 884−892.
(110) Spackova, N.; Berger, I.; Egli, M.; Sponer, J. *J. Am. Chem. Soc.* **1998**, *120*, 6147−6151.
(111) Yildirim, I.; Stern, H. A.; Sponer, J.; Spackova, N.; Turner, D. H. *J. Chem. Theory Comput.* **2009**, *5*, 2088−2100.
(112) Calladine, C. R. *J. Mol. Biol.* **1982**, *161*, 343−352.
(113) Dickerson, R. E. *Biophys. J.* **1983**, *41*, A210−A210.
(114) Egli, M.; Portmann, S.; Usman, N. *Biochemistry* **1996**, *35*, 8489−8494.
(115) Auffinger, P.; Westhof, E. *J. Biomol. Struct. Dyn.* **1998**, *16*, 693−707.
(116) Sundaralingam, M.; Pan, B. C. *Biophys. Chem.* **2002**, *95*, 273−282.
(117) Adamiak, D. A.; Milecki, J.; Adamiak, R. W.; Rypniewski, W. *New J. Chem.* **2010**, *34*, 903−909.
(118) Cerutti, D. S.; Freddolino, P. L.; Duke, R. E.; Case, D. A. *J. Phys. Chem. B* **2010**, *114*, 12811−12824.

(119) Dock-Bregeon, A. C.; Chevrier, B.; Podjarny, A.; Johnson, J.; Debear, J. S.; Gough, G. R.; Gilham, P. T.; Moras, D. *J. Mol. Biol.* **1989**, *209*, 459−474.
(120) Mooers, B. H. M.; Singh, A. *RNA* **2011**, *17*, 1870−1883.
(121) Bullock, S. L.; Ringel, I.; Ish-Horowicz, D.; Lukavsky, P. J. *Nat. Struct. Mol. Biol.* **2010**, *17*, 703−709.
(122) Sprous, D.; Young, M. A.; Beveridge, D. L. *J. Phys. Chem. B* **1998**, *102*, 4658−4667.
(123) Noy, A.; Perez, A.; Laughton, C. A.; Orozco, M. *Nucleic Acids Res.* **2007**, *35*, 3330−3338.
(124) Lankas, F.; Spackova, N.; Moakher, M.; Enkhbayar, P.; Sponer, J. *Nucleic Acids Res.* **2010**, *38*, 3414−3422.
(125) Pan, Y. P.; MacKerell, A. D. *Nucleic Acids Res.* **2003**, *31*, 7131−7140.
(126) Reblova, K.; Fadrna, E.; Sarzynska, J.; Kulinski, T.; Kulhanek, P.; Ennifar, E.; Koca, J.; Sponer, J. *Biophys. J.* **2007**, *93*, 3932−3949.
(127) Deng, N. J.; Cieplak, P. *J. Chem. Theory Comput.* **2007**, *3*, 1435−1450.
(128) Hobza, P.; Kabelac, M.; Sponer, J.; Mejzlik, P.; Vondrasek, J. *J. Comput. Chem.* **1997**, *18*, 1136−1150.